Therapeutic effects of bee venom and its major component, melittin, on atopic dermatitis *in vivo* and *in vitro*

Running Title: Effects of bee venom and melittin on atopic eczema

Hyun-Jin An[1], Jung-Yeon Kim[1], Woon-Hae Kim[1], Mi-Gyeong Gwon[1], HyeMin Gu[1], MinJi Jeon[1], Sang-Mi Han[2], Sok Cheon Pak[3], Chong-Kee lee[4], InSook Park[5], and Kwan-Kyu Park[1*]

[1]Department of Pathology, College of Medicine, Catholic University of Daegu, 33, Duryugongwon-ro 17-gil, Nam-gu, Daegu, 42472, Republic of Korea

[2]Department of Agricultural Biology, National Academy of Agricultural Science, RDA, 300, Nongsaengmyeong-ro, Wansan-gu, Jeonju-si, Jeollabuk-do 54875, Republic of Korea

[3]School of Biomedical Sciences, Charles Sturt University, Panorama Avenue, Bathurst, NSW 2795, Australia

[4]Department of Immunology, College of Medicine, Catholic University of Daegu, 33, Duryugongwon-ro 17-gil, Nam-gu, Daegu, 42472, Republic of Korea

[5]Department of Oral and Maxillofacial Surgery, Department of Dentistry, College of Medicine, Catholic University of Daegu, 33, Duryugongwon-ro 17-gil, Nam-gu, Daegu, 42472, Republic of Korea

Corresponding author:
Kwan-Kyu Park, M.D., Ph.D
Department of Pathology, College of Medicine, Catholic University of Daegu, 33, Duryugongwon-ro 17-gil, Nam-gu, Daegu, 42472, Republic of Korea
Tel: (+82)53-650-4149, Fax: (+82)53-650-4834, E-mail: kkpark@cu.ac.kr

This article has been accepted for publication and undergone full peer review but has not been through the copyediting, typesetting, pagination and proofreading process which may lead to differences between this version and the Version of Record. Please cite this article as doi: 10.1111/bph.14487

This article is protected by copyright. All rights reserved.

Accepted Article

Abstract

Background and purpose

Atopic dermatitis (AD) is a multifactorial skin disease with complex interactions of innate and adaptive immune responses based on a genetic, pharmacological, and psychological predisposition. There are several treatment approaches for AD, including topical glucocorticosteroids, emollients, phototherapies, calcineurin inhibitors, and immunosuppressants, such as cyclosporine A. These therapies reduce inflammation, but they also cause various side effects. Therefore, it is necessary to develop new therapeutic approaches for AD treatment without side effects. There are several studies on natural materials or toxins, such as herbs, ginseng extract, and snake venom, for AD treatment. However, bee venom (BV) and melittin (Mel)-mediated AD treatment has rarely been studied.

Experimental approach

The present study was designed to determine the effect of BV and Mel in an AD-like model. This study investigated the potential pharmacological effects of BV and its major component, Mel, on 1-Chloro-2,4-dinitrobenzene (DNCB)-induced *in vivo* and TNF-α/IFN-γ-induced *in vitro* AD-like skin disease models.

Key results

We found that BV and Mel possess potent anti-atopic activities, as evidenced by decreased DNCB-induced AD-like skin lesions in an animal model. *In vitro* studies using TNF-*α*/IFN-*γ*-stimulated human keratinocytes revealed that BV and Mel inhibited the exaggerated expression of chemokines, such as TARC/CCL17 and MDC/CCL22, and pro-inflammatory cytokines, including IL-1β, IL-6, and IFN-γ, through the blockade of the NF-κB and STAT signaling pathways.

Conclusions and implications

In conclusion, these results suggest that BV and Mel would be suitable for epicutaneous application, as topical administration is often appropriate for the treatment of AD.

Accepted Article

This article is protected by copyright. All rights reserved.

1. JAK2 (Janus kinase 2)

Target Id: 2048

2. STAT3 (signal transducer and activator of transcription 3)

Target Id: 2994

Abbreviations

AD: atopic dermatitis

BV: bee venom

CCK: cell counting kit

DNCB: 1-Chloro-2,4-dinitrobenzene

ELISA: enzyme-linked immunosorbent assay

EMSA: Electrophoric mobility shift assay

GAPDH: glyceraldehyde-3-phosphate dehydrogenase

IFN: interferon

IgE: immunoglobulin E

IL: interleukin

JAK: janus kinase

MDC/CCL22: macrophage-derived chemokine

Mel: melittin

NF-κB: nuclear factor κ-light-chain-enhancer of activated B cells

RBC: red blood cell

Accepted Article

This article is protected by copyright. All rights reserved.

RT: room temperature

STAT: signal transducer and activator of transcription

TARC/CCL17: thymus and activation regulated chemokine

Th cell: helper T cell

TNF: tumor necrosis factor

TSLP: thymic stromal lymphopoietin

Introduction

Atopic dermatitis (AD), commonly known as atopic eczema, is a multifactorial skin disease, with complex interactions of innate and adaptive immune responses based on a genetic, pharmacological, and psychological predisposition (Boguniewicz and Leung, 2011). AD, which is one of the most common chronic inflammatory skin diseases, is characterized by an impaired epidermal barrier, eczematous lesions, pruritus, dry skin, an abnormal immune response, and an immunoglobulin (Ig)E-mediated allergy to various exogenous antigens (Lee and Lee, 2014). The pathogenesis of AD involves a complex inflammatory process (Tan and Corren, 2011). Two competing hypotheses are generally presented regarding the pathogenesis of AD. The first proposes a primary immune functional disorder, resulting in IgE sensitization and a subsequent epithelial-barrier obstruction (Nair and Peate, 2015). The second suggests that a disturbance of the skin barrier, either caused by an intrinsic genetic deficiency in epidermal skin barrier formation or as a result of an environmental transition, leads to atopic disease (Brandt and Sivaprasad, 2011). While debate around these theories remains, it is obvious that a number of genetic and environmental factors contribute to skin barrier dysfunction and immune dysregulation in AD (Blakely et al., 2016).

The first hypothesis of AD pathogenesis invokes an imbalance between helper T (Th) cells 1 and 2 by the presence of a specific IgE response in association with Th2 immune responses (Choi and Kim, 2013). In healthy individuals, balance exists among important subsets of helper T cells (e.g., Th1, Th2, Th17, and Th22). The pathogenesis of acute AD is related to Th2-dominant inflammation, characterized by the dermal infiltration of Th cells, macrophages, and eosinophils, increase in allergen-specific IgE, mast cell activation, and Th2 cytokine production (Mizutani et al., 2015). Th2 cells secrete cytokines, interleukin (IL)-4

This article is protected by copyright. All rights reserved.

and IL-5, that upregulate antibody formation via B cells, eosinophils, mast cells, and other pathways (Kidd, 2003). IL-4 and IL-13 have established roles in B cell differentiation and class switching, thus providing a link to characteristic elevations of serum IgE levels in AD, as well as eosinophil and mast cell infiltration into the skin (Chan et al., 2013). The pathogenesis of chronic AD is related to predominant Th1 cells and interferon (IFN)-γ, and chronic AD skin lesions undergo tissue remodeling caused by chronic inflammation (Coondoo, 2012). There are also increased numbers of mast cells but virtually no accumulation of neutrophils. Th1 cells secrete the cytokine IFN- γ and activate inflammatory pathways mainly via macrophage activation (Kidd, 2003).

The second hypothesis, epidermal barrier dysfunction, involves dry, itchy skin, which is exacerbated by a mechanical injury inflicted by scratching. This enables the entry of antigens via the skin to result in the production of inflammatory cytokines (Oyoshi et al., 2009). A number of the barrier genes are localized on chromosome 1 in a cluster epidermal differentiation complex and include filaggrin, loricrin, and involucrin. During the transition from stratum granulosum to stratum corneum, profilaggrin is cleaved into multiple filaggrin monomers that provide physical strength by aggregating the keratin bundles (Kalinin et al., 2002). Loss-of-function mutations in the filaggrin gene have been identified as the main genetic predisposing factor for AD and multiple other allergic diseases, including asthma (Irvine et al., 2011). According to the findings of the filaggrin-deficient mice experiments, skin barrier function depends on the normal differentiation of keratinocytes (Kawasaki et al., 2012). Thus, keratinocytes as the major group of epidermal cells, play an important role in the pathogenesis of inflammatory skin diseases, such as AD (Jung et al., 2012).

Many commercial formulations for the treatment of AD are available in gels, creams, lotions, or ointments but show limited effectiveness (Shah et al., 2012). Furthermore, there are several treatment approaches for AD, such as topical glucocorticosteroids, emollients, phototherapies, calcineurin inhibitors, and immunosuppressants, such as cyclosporine A (Misery, 2011, Berke et al., 2012). These therapies reduce inflammation, but they also cause various side effects. For example, topical steroid therapy is the most effective remedy for AD, but the continual repetitive application of steroids leads to side effects that include skin thinning and atrophy (Del Rosso and Friedlander, 2005). Therefore, the development of new therapeutic approaches without side effects is necessary for AD treatment. There are several studies on natural materials or toxins, such as herbs, ginseng extract, and snake venom, for

This article is protected by copyright. All rights reserved.

AD treatment (Park et al., 2016, Sohn et al., 2011). A recent study investigated the effects of bee venom (BV) phospholipase A2 on house dust mite extract-induced AD-like skin lesion in mice (Jung et al., 2017). However, beneficial effect of BV on AD has not been clearly recognized.

Purified BV is a natural toxin produced by honeybees (*Apis mellifera*) and has been extensively used as a traditional medicine for various diseases (Son et al., 2007). BV contains various peptides, including melittin (Mel), apamin, adolapin, and mast cell degranulating peptide along with enzymes, biological amines, and nonpeptide components (Lariviere and Melzack, 1996). Mel, the major component (50% of dry weight) of BV, is a small linear peptide composed of 26 amino acids. Several studies have examined the biological and pharmacological activities of BV and Mel, confirming that they possess radioprotective, anti-inflammatory, anti-bacterial, anti-viral, and anti-cancer activities (Raghuraman and Chattopadhyay, 2007, Lee and Bae, 2016). In addition, it has pain-relief effects, anti-rheumatoid arthritis effects, and aids immune modulatory activity (An et al., 2016). A recent study investigated the effects of Mel on *Propionibacterium acnes*-induced inflammatory responses *in vitro* and *in vivo* (Lee et al., 2014). However, the precise mechanism by which BV and Mel are thought to act in AD is not fully understood. Based on the various physiological activities of BV and Mel, they are thought to be effective in AD. The excellent anti-inflammatory effect of BV and Mel, which is associated with inflammatory skin disease, is expected to maximize the effects of BV and Mel.

Therefore, the present study was designed to determine the effect of BV and Mel in an AD-like model. Consequently, this study investigated the potential pharmacological effects of BV and its major component, Mel, on 1-Chloro-2,4-dinitrobenzene (DNCB)-induced *in vivo* and tumor necrosis factor (TNF)-α/IFN-γ-induced *in vitro* AD-like skin disease models.

Accepted Article

This article is protected by copyright. All rights reserved.

Methods

Animal

Six-week-old female Balb/c mice (18-23 g; Samtoko, Gyeonggi-do, Korea) were individually housed in polycarbonate animal cages and maintained under a constant temperature (22 ± 2°C) and humidity (55%). The mice had free access to water and food and were subjected to 12 h light-dark cycles. After 1 week of acclimatization, the Balb/c mice were randomly divided into nine groups (n = 5 per group) as follows: (1) an untreated group (normal control, NC); (2) a DNCB (1-chloro-2,4-dinitrobenzene; Sigma)-sensitized and challenged group (DNCB); (3) a DNCB-sensitized and challenged group with 0.1 g placebo treated group (Pla); (4-6) DNCB-sensitized and challenged groups with 100, 200, and 500 μg of BV in mixed with placebo (the groups were named BV100, BV200, and BV500); (7-9) DNCB-sensitized and challenged groups with 100, 200, and 500 μg of Mel in mixed with placebo (Mel100, Mel200, and Mel500). Concentration of BV and Mel were estimated based on previous studies (Lee et al., 2014). All animal care and experimental procedures were carried out strictly in accordance with the criteria of the 'Institutional Animal Care and Use Committee of Catholic University of Daegu' and were approved by the 'Institutional Animal Care and Use Committee of Catholic University of Daegu' (Daegu, Korea; Approval number DCIAFCR-151007-9-Y and DCIAFCR-160428-Y). The animals were treated humanely, and all efforts were made to minimize the animals' suffering and the animal numbers. Animal studies are reported in compliance with the ARRIVE guidelines (McGrath and Lilley, 2015).

Cell cultures

The human keratinocyte HaCaT cell line was cultured in high glucose Dulbecco's Modified Eagle's Medium supplemented with 10% (v/v) fetal bovine serum and antibiotics (100 U · mL^{-1} penicillin and 100 μg · mL^{-1} streptomycin) at 37°C in a humidified 5% CO_2 incubator. HaCaT (5.0×10^5 cells · mL^{-1}) cells were seeded in the complete medium. Twenty-four hours later, the medium was changed to serum-free medium conditions with BV (1, 10, and 100 ng · mL^{-1}; Sigma, St. Louis, MO, USA) and Mel (0.1, 0.5, and 1 μg · mL^{-1}; Enzo, Plymouth, PA, USA). After 30 min, the cells were stimulated with 10 ng · mL^{-1} TNF-α/IFN-γ for 9 h. PBS (pH 7.4), FBS, DMEM, penicillin, and streptomycin were purchased from Gibco (Grand

This article is protected by copyright. All rights reserved.

Island, NY, USA). Recombinant human TNF-α and IFN-γ were purchased from R&D Systems (Minneapolis, MN, USA).

AD mice model

The mice were anesthetized by isoflurane inhalation (Ifran; HANA Pharm, Seoul, Korea) by using RC2 Rodent Circuit Controller (VETEQUIP, CA, USA). During anesthesia, dorsal skin was shaved with an electric clipper and hair removal creams. After 24 h, Balb/c mice were sensitized with 200 μL of 1% DNCB in an acetone:olive oil (3:1) solution on their shaved dorsal skin twice each week for a week. Mice were then challenged with 200 μL of 0.4% DNCB twice a week for five weeks (Choi et al., 2013, Chan et al., 2013). Two weeks after the first induction of skin inflammation, BV and Mel (100, 200, and 500 μg mixed with a placebo) were applied to the dorsal skin five times per week for four weeks. The animal model of atopic dermatitis in this paper was based on the 'Guideline for the efficacy of herbal medicinal herb medicine-Atopic dermatitis' of South Korea Ministry Food and Drug Safety. The experimental protocol used in the present study is depicted schematically in Figure 1A. At the end of each treatment period, blood samples were collected by cardiac puncture from the mice, and the mice were sacrificed by CO_2 asphyxiation. After sacrifice, their dorsal skins were excised for the next experiments. Blood samples were allowed to clot for 1 h at room temperature (RT) before centrifuging for 20 min at 13000 rpm. The serum was prepared from the blood samples and stored at -70°C for further analysis. After blood collection, dorsal skins were excised.

Histological analysis

All skin tissue specimens were fixed in 10% formalin for 24 h at RT. After fixation, perpendicular sections to the anterior–posterior axis of the dorsal skin were dehydrated in graded ethanol, cleared in xylene, and embedded in paraffin. The sections (4 μm) were mounted on glass slides, rehydrated to distilled water, and stained with Hematoxylin and eosin (H&E). As part of the histological assessment, all slides were examined under a slide scanner (3DHISTECH Pannoramic MIDI, Budapest, Hungary). The thickness of the

This article is protected by copyright. All rights reserved.

epidermis and dermis was analyzed with iSolution DT software (IMT i-Solution, Burnaby, BC, Canada).

Mast cell infiltration and degranulation

After mice were sacrificed, the DNCB-injected site (1 × 1 cm) was excised, fixed in formalin for 24 h, and embedded in paraffin. Deparaffinized skin sections were stained with Giemsa for histological analysis. To measure the mast cell infiltration and degranulation, each slide was counted from all fields per section at 400x magnification. As part of the histological assessment, all slides were examined under a slide scanner. The granulation index per single mast cell was calculated by dividing the total number of degranulation from the total mast cells.

Enzyme-linked immunosorbent assay (ELISA)

The mice serum levels of IgE (Bethyl Laboratories, Montgomery, TX, USA), IL-4, IFN-γ and thymic stromal lymphopoietin (TSLP, R&D Systems, Minneapolis, MN, USA) were measured using-ELISA kits according to the manufacturer's instructions. Reading of the absorbance at 450 nm was done using an ELISA reader (BMG Labtech, Ortenaukreis, Germany).

Preparation of splenocytes

The spleen was aseptically removed from each group of Balb/c mice, and a single-cell suspension was prepared by forcing the spleen through a 71 μm stainless steel mesh. Red blood cells (RBCs) were lysed using RBC lysis buffer (Qiagen, Hilden, Germany), and the lysate was centrifuged at 1500 × g for 10 min at 4°C. Splenocytes were suspended in RPMI 1640 (Invitrogen, Carlsbad, CA, USA) medium supplemented with 10% FBS, 100 U · mL^{-1} penicillin, and 100 mg · mL^{-1} streptomycin, and spleen cells (5.0×10^5 cells/well) were seeded in plates for each group and incubated for 72 h. Supernatants were harvested and

This article is protected by copyright. All rights reserved.

measured for IgE using ELISA kits.

Preparation of total and nuclear protein from HaCaT cells

For total protein assays, cells were lysed in lysis reagent (Cell Lytic™ M, Sigma-Aldrich, St. Louis, MO, USA), according to the instruction manual. The protein concentration of the samples was measured with Bradford assay (Bio-Rad Laboratories, Hercules, CA, USA), with the optimal density at 595 nm, by using a spectrophotometer. Nuclear and cytosol protein were collected using NE-PER nuclear and cytoplasmic extraction reagent kits (Thermo Fisher Scientific, Waltham, MA, USA) according to the manufacturer's instructions. All protein concentrations were quantified using the Bradford protein assay.

Western blot analysis

The protein samples were separated on precast gradient polyacrylamide gels (Bolt™ 4-12% Bis-Tris Plus Gels, Thermo Fisher Scientific) and transferred to nitrocellulose membranes (GE Healthcare) by using Bolt™ Mini Blot Module and Mini Gel Tank (Thermo Fisher Scientific), according to the manufacturer's recommendations. The membrane was blocked in 5% bovine serum albumin. The blocked membrane was probed with a primary antibody and horseradish peroxidase-conjugated secondary antibody. Following a repeat of the wash step, the membrane was kept in enhanced chemiluminescence detection reagents (Thermo Fisher Scientific) for 1 min. Signal intensity was measured with an image analyzer (ChemiDoc™ XRS+ system, Bio-Rad Laboratories). The primary antibodies used were anti-IL-1β (Santa Cruz Biotechnology, Santa Cruz, CA, USA), anti-IL-6 (Abcam, Cambridge, MA, USA), anti-IFN-γ (Abcam), anti-glyceraldehyde-3-phosphate dehydrogenase (GAPDH), anti-Janus kinase (JAK)2, anti-phospho-JAK2, anti-signal transducer and activator of transcription (STAT) 1 and 3, anti-phospho-STAT1 and 3, anti-IKKα, anti-phospho-IKKα, anti-IκBα, anti-phospho-IκBα, anti-nuclear factor κ-light-chain-enhancer of activated B cells (NF-κB), and anti-phospho-NF-κB p65 were purchased from Cell Signaling Technology (Beverly, MA, USA). In addition, anti-Lamin B from Invitrogen was used.

This article is protected by copyright. All rights reserved.

Quantitative real-time PCR

Total mRNA was extracted from the dorsal skin and HaCaT cell by using TRIzol reagent (Thermo Fisher Scientific), according to the manufacturer's recommendations. Reverse transcription reaction was performed with AccuPower RT Premix and Oligo dT18 (Bioneer, Daejeon, Korea), according to manufacturer's instructions. Real-time PCR was performed in a LightCycler nano System (Roche Applied Science, Mannheim, Germany) using a LightCycler DNA Master SYBR Green I (Roche Applied Science). PCR mixtures contained 100 ng of cDNA and 0.5 μM each of forward and reverse primers. The samples were denatured at 95°C for 10 min, followed by 45 cycles of annealing and extension at 95°C for 20 s, 60°C for 20 s, and 72°C for 20 s. Expression values were normalized to GAPDH. Quantitative real-time PCR products were further confirmed by melting curve analysis. The primer sequences were as follows: IFN-γ, forward, 5'-TGG CAT AGA TGT GGA AGA AAA GAG-3', and reverse, 5'-TGC AGG ATT TTC ATG TCA CCA T-3'; IL-4, forward, 5'-ACAGGAGAAGGGACGCCAT-3', and reverse, 5'-GAAGCCCTACAGACGAGCTCA-3'; TARC/CLL17, forward, 5'-AGG GAC CAC ACA GAG AC-3', and reverse, 5'-CTC GAG CTG CGT GGA TGT GC-3'; MDC/CCL22, forward, 5'-ATG GCT CGC CTA CAG ACT GCA CTC-3', and reverse, 5'-CAC GGC AGC AGA CGC TGT CTT CCA-3'; GAPDH, forward, 5'- GGA GCC AAA AGG GTC ATC AT-3', and reverse, 5'-GTG ATG GCA TGG ACT GTG GT-3'.

Immunohistochemical staining

Paraffin-embedded tissue sections at 4 μm thicknesses were deparaffinized with xylene, dehydrated in gradually diminishing concentrations of ethanol, and treated with 3% hydrogen peroxidase in methanol for 10 min to block endogenous peroxidase activity. The tissue sections were immersed in a 10 mM sodium citrate buffer (pH 6.0) for 5 min at 95°C. The last step was repeated using a 10 mM sodium citrate solution (pH 6.0). The sections stayed in the same solution while cooling for 20 min, and they were rinsed in PBS. The sections were then incubated with a primary antibody (1:100 dilution) for 1 h at 37°C. The primary antibodies were as follows: anti-TSLP, anti-CD3, and anti-CD4 (Abcam). The signal was visualized using an Envision System (DAKO, CA, USA) for 30 min at 37°C. 3,3'-diaminobenzidine

This article is protected by copyright. All rights reserved.

tetrahydrochloride (DAB) was used as the coloring reagent, and hematoxylin was used as the counter-stain. The slides were examined with a slide scanner, Pannoramic MIDI, and analyzed with iSolution DT software.

Immunofluorescence staining and confocal microscopy

The paraffin-embedded skin tissue sections were deparaffinized with xylene and dehydrated in gradually decreasing concentrations of ethanol. The tissue sections were then placed in a blocking serum (5% bovine serum albumin in PBS) at RT for 1 h. A primary antibody (1:500 dilution) was incubated at RT for 2 h, and a secondary antibody incubation (1:200 dilution) was performed at RT for 1 h. The antibodies included filaggrin (Abcam) and a goat anti-rabbit secondary antibody conjugated with Alexa Fluor 488 (Thermo, MA, USA). Sections were then counterstained with Hoechst 33342. The slides were mounted using a VECTASHIELD Mounting Medium (VECTOR Laboratories, Burlingame, CA, USA). Stained slides were viewed under a confocal microscope system (Nikon A1 microscope equipped with a digital camera, Nikon, Tokyo, Japan).

HaCaT cell were seeded at a density of 2.0×10^5 cells/well in 2-well chamber slide (Eppendorf, Hamburg, Germany). After 24 h, the medium was changed to a serum-free medium containing the indicated concentration of BV (1, 10, and 100 ng · mL^{-1}) and Mel (0.1, 0.5, and 1 μg · mL^{-1}). After 2 h, the cells were co-treated with 10 ng · mL^{-1} TNF-α/IFN-γ for 1 h. The treated cells were washed with PBS and fixed with 4% paraformaldehyde for 20 min at RT. Fixed cells were treated with 0.1% Triton X-100 in PBS for 2 min to permeabilize. Following permeabilization, the cells were blocked in PBS containing 5% bovine serum albumin at RT for 1 h. After blocking, the cells were incubated with diluted primary antibody overnight at 4℃, and the reaction with secondary antibody was performed at RT for 2 h. The nuclei were stained with Hoechst 33342 solution for 10 min at 37℃. Slides were mounted using fluorescence mounting medium (Dako, CA, USA). Specimens were examined and photographed using a confocal microscope system. The antibodies used are as follows: anti-phospho-STAT1, anti-phospho-STAT3, anti-F-actin, and anti-mouse-biotinylated, and anti-rabbit-biotinylated secondary antibodies conjugated with Alexa Fluor 488 of Alexa Fluor 555.

This article is protected by copyright. All rights reserved.

Cell viability assays

The cell viability of HaCaT was detected using cell counting kit (CCK)-8 assays (Dojindo, Kumamoto, Japan). The HaCaT cells were seeded in 96-well plate at 5.0×10^4 cells · mL^{-1} and allowed to attach for 24 h. The medium was replaced with serum-free media. Cells were treated with serum-free media containing different concentration of BV (1, 10, and 100 ng · mL^{-1}) and Mel (0.1, 0.5, and 1 μg · mL^{-1}) for 9, 12, and 24 h. After experimental treatment, 10 μl of WST-8 solution (2-(2-methoxy-4-nitrophenyl)-3-(4-nitrophenyl)-5-(2,4-disulfophenyl)-2H-tetrazolium, monosodium salt) was added to each well, and the HaCaT cells were incubated for an additional 2-4 h at 37℃. The absorbance values were measured at 450 nm using a microplate reader.

Electrophoric mobility shift assay (EMSA)

Lightshift® Chemiluminescent EMSA Kit (Thermo) was used for the EMSA assay, according to the manufacturer's instructions. The image analyzer (Chemidoc XRS+ system) was used to detect the chemiluminescence of biotin-labeled DNA. The NF-κB (5'-AGT TGA GGG GAC TTT CCC AGG C-3′) oligonucleotide probe was end-labeled with DIG-ddUTP.

Statistical analysis

All data are presented as means ± standard error of the mean (SEM). Statistical significance was tested using GraphPad Prism 5 (GraphPad Software, Inc., San Diego, CA, USA) one-way analysis of variance with Tukey's multiple comparison test. Differences with $p < 0.05$ were considered significant.

Nomenclature of Targets and Ligands

Key protein targets and ligands in this article are hyperlinked to corresponding entries in http://www.guidetopharmacology.org, the common portal for data from the IUPHAR/BPS

This article is protected by copyright. All rights reserved.

Guide to PHARMACOLOGY (Southan et al., 2016), and are permanently archived in the Concise Guide to PHARMACOLOGY 2017/18 (Alexander et al., 2017).

Accepted Article

Results

DNCB is capable of inducing AD-like skin diseases in a mouse model

DNCB is known to induce AD-like skin lesions. When compared to day 0 corresponding to the induction period of skin inflammation, the DNCB-treated mice showed significantly increased physical signs of AD, such as pruritus, edema, erythema, scarring, and excoriation, during a three-week period (Figure 1B). Histopathological analysis confirmed that DNCB induced mast cell accumulation and degranulation (shown as arrows in the figure) in the dorsal skin (Figure 1C).

BV and Mel alleviated DNCB-induced inflammations and mast cells into AD-like skin lesions in an animal model

AD-like skin lesions are characterized by epidermal and dermal thickening, the dermal infiltration of $CD4^+$ T cells, and the local expression of Th2 cytokines (Fröhlich et al., 2009). Therefore, we investigated the effects of BV and Mel on DNCB-induced AD-like symptoms and responses using H&E staining. BV and Mel treatment significantly decreased the dorsal skin thickness compared with that of the DNCB group (Figure 2B, Supplementary Figure S1B). Histological analysis confirmed that BV and Mel inhibited pathological changes including the infiltration of inflammatory cells in skin lesions (Figure 2A, Supplementary Figure S1A). Mast cells have been linked to the pathophysiology of allergic disorders, including AD (Galli and Tsai, 2012). According to the evaluation of mast cell infiltration and degranulation using Giemsa staining, the mast cell infiltration and degranulation in skin lesions was increased in the DNCB group, while the topical application of BV and Mel resulted in the decreased infiltration and degranulation of mast cells (Figure 3, Supplementary Figure S2).

This article is protected by copyright. All rights reserved.

Effects of BV and Mel on mice serum IFN-γ, IL-4, IgE, and TSLP

AD is characterized by two distinct phases, the chronic and acute phases, resulting in either Th1- or Th2-dominant inflammation (Kim et al., 2015). Th1-specific signature cytokines IFN-γ and TNF-α activate mononuclear phagocytes including macrophages, which are implicated in organ-specific autoimmunity by the infection of intracellular pathogens, such as bacteria and protozoa (Guo et al., 2009). In contrast, IL-4 is associated with the Th2 response. Therefore, this study investigated whether BV and Mel affected the Th1 or Th2 responses in an AD-like Balb/c mouse model. The levels of IFN-γ, IL-4, IgE, and TSLP in the serum increased in response to DNCB treatment relative to normal control mice. However, treatment with BV and Mel markedly decreased the serum IFN-γ, IL-4, IgE, and TSLP levels in DCNB-sensitized Balb/c mice (Figure 4A, Supplementary Figure S3A). The effect of Mel on DNCB-induced IgE change in splenocytes was further investigated. The concentration of IgE in the spleen tissue of the DNCB-treated group mice was increased, but this increase was inhibited by Mel in both the 200 and 500 μg dose groups (Figure 4B). Next, we examined whether BV and Mel could regulate immune responses. Real-time PCR was used to measure the gene expression of IFN-γ and IL-4. The mRNA expression levels of IFN-γ and IL-4 in the skin of the DNCB-treated group mice were increased, but this increase was inhibited by BV and Mel in the 100 and 500 μg doses, respectively (Figure 4C, Supplementary Figure S3B).

Effects of BV and Mel on TSLP expression, $CD4^+$, and $CD3^+$ T cells in DNCB-sensitized mice

TSLP expression plays an important role in regulating Th2 cell-mediated immunity and AD. In addition, environmental stimuli trigger keratinocytes for the production of TSLP with the subsequent activation of dendritic cells, epithelial cells, and mast cell, which results in Th2-type allergic immune responses (Lee et al., 2011). Treatment with BV and Mel significantly inhibited the DNCB-induced expression of TSLP, suggesting that BV and Mel have the potential to regulate Th2 cell-mediated immunity in the epidermis. Since TSLP expressions appear distinctly localized in the extracellular and cytoplasmic domains of the epidermal layer, they seem to be triggered by keratinocytes. The infiltration of $CD4^+$ T cells and the up-regulation of Th2 cytokines are typical features of AD lesions (Choi et al., 2013). We

This article is protected by copyright. All rights reserved.

performed immunohistochemical and histological analysis to examine whether BV and Mel reduced the levels of $CD4^+$ and $CD3^+$ T cells, respectively, in the dorsal skin. The levels of $CD4^+$ and $CD3^+$ T cells in DNCB-induced AD lesions in mice were higher than those in normal mice. BV and Mel, however, decreased the levels of $CD4^+$ and $CD3^+$ (Figure 5A and B, Supplementary Figure S4A and B) T cells in the dorsal skin.

BV and Mel improve abnormal epidermal differentiation

Filaggrin-related barrier disruption can be a primary cause of AD (Elias and Schmuth, 2009). Th2 cytokines, such as IL-4, IL-13, and IL-22, have been implicated in the downregulation of filaggrin expression in AD-induced lesions (Jung et al., 2014). We investigated the therapeutic effects of BV and Mel on abnormal the epidermal differentiation. The apparent decrease in the filaggrin level shown as the expression of the epidermal differentiation marker using immunofluorescence staining after DNCB stimulation was reversed with BV and Mel treatment (Figure 5C, Supplementary Figure S4C).

Effects of BV and Mel on pro-inflammatory chemokines and cytokines in TNF-α/IFN-γ-stimulated HaCaT cells

To investigate the cytotoxicity of BV and Mel, CCK-8 assay was performed to analyze the cell viability of the HaCaT cell line. Cells were treated with BV and Mel at different concentrations and assessed at different time points. Keratinocytes were relatively stable with no significant change in viability up to 9 h. Cells treated with 100 ng · mL^{-1} BV and 1 μg · mL^{-1} Mel showed a significant decrease in viability by approximately 10-15% at 24 h compared to no treatment (Figure 6A, Supplementary Figure S5A). These data suggest that BV and Mel had no cytotoxicity to HaCaT cells up to 9 h. Accordingly, 9 h cell culture was used in subsequent in vitro experiments. AD lesions are capable of producing TARC/CCL17 and MDC/CCL22 through the activated keratinocytes (Brandt and Sivaprasad, 2011). As such, a decrease in the production of TARC/CCL17 and MDC/CCL22 in keratinocytes may be an effective target for AD treatment (Qi et al., 2009). Therefore, we investigated the effects of BV and Mel on TNF-α/IFN-γ-induced pro-inflammatory chemokine expression in HaCaT

This article is protected by copyright. All rights reserved.

cells. TNF-α/IFN-γ treatment significantly induced the mRNA expression of TARC/CCL17 and MDC/CCL22, which were significantly inhibited by BV and Mel treatment (Figure 6C, Supplementary Figure S5C). Consistent with these findings, TNF-α/IFN-γ treatment significantly provoked the release of IL-1β, IL-6, and IFN-γ from HaCaT cells. However, BV and Mel treatment significantly inhibited TNF-α/IFN-γ-induced pro-inflammatory cytokine secretion (Figure 6B, Supplementary Figure S5B). These results suggest that BV and Mel can modulate the expression of chemokines via the suppression of pro-inflammatory cytokines in TNF-α/IFN-γ-stimulated HaCaT cells.

Effects of BV and Mel on JAK/STAT signal pathways in TNF-α/IFN-γ-activated HaCaT cells

The JAK/STAT pathway plays a critical role in the disruption of the epidermis barrier function and can be a therapeutic target in AD (Amano et al., 2015). In addition, cytokine-mediated activation of STAT proteins plays an essential role in $CD4^+$ T cell differentiation and the regulation of immune responses (O'Shea et al., 2011). We addressed the effects of BV and Mel on JAK/STAT signaling. HaCaT cells were incubated in the presence or absence of BV and Mel for 2 h and then simulated with TNF-α/IFN-γ for 1 h. Cytosolic and nuclear fractions were evaluated for the expression of JAK2, STAT1, and STAT3 by Western blotting analysis. The phosphorylation of JAK2 and nuclear translocation of p-STAT1 and p-STAT3 were highly increased by TNF-α/IFN-γ treatment. However, treatment with BV and Mel decreased the levels of p-JAK2 as well as the nuclear translocation of p-STAT1 and p-STAT3 (Figure 7A, Supplementary Figure S6A). The suppressed phosphorylation of JAK2, STAT1, and STAT3 from BV and Mel treatment was further confirmed by immunofluorescence stain. When cells were treated with BV (100 ng · mL^{-1}) and Mel (1 μg · mL^{-1}), STAT1 and STAT3 were predominantly localized in the cytoplasm, rather than in the nucleus, suggesting a role of STAT1 and STAT3 as transcriptional activators (Figure 7B, Supplementary Figure S6B). The inhibition of these signaling pathways by BV and Mel could be responsible for the decrease in the production of pro-inflammatory chemokines and cytokines.

This article is protected by copyright. All rights reserved.

Effects of BV and Mel on NF-κB pathways in TNF-α/IFN-γ-stimulated HaCaT cells

TNF-α/IFN-γ induces the production of chemokines and cytokines in keratinocytes by activating NF-κB (Ju et al., 2009). The NF-κB signaling pathway contributes to the production of TARC/CCL17 and MDC/CCL22 in TNF-α/IFN-γ-stimulated HaCaT cells (Qi et al., 2012). Accordingly, we focused our analysis on IKK, IκB, and NF-κB in TNF-α/IFN-γ-stimulated HaCaT cells, as shown in Figure 7C, Supplementary Figure S6C, TNF-α/IFN-γ treatment significantly increased the phosphorylation of cytosolic IκB, and NF-κB and nuclear p-NF-κB. However, BV and Mel treatment decreased the phosphorylation levels of IκB, and NF-κB in a dose-dependent manner. To further evaluate the effects of BV and Mel on NF-κB DNA-binding activity in HaCaT cells, nuclear extracts were analyzed by EMSA (Figure 7D, Supplementary Figure S6D). TNF-α/IFN-γ caused increased the NF-κB DNA-binding activity in HaCaT cells. In contrast, this increased binding activity was markedly withdrawn after treatment with BV and Mel. These results suggest that the inhibition of TNF-α/IFN-γ-induced TARC/CCL17 and MDC/CCL22 chemokine production by BV and Mel is mediated by the suppression of both NF-κB and STAT1 and STAT3 activation.

Discussion

AD is the most common allergic inflammatory skin disease (Sugiura et al., 2003). Interactions of genetic, environmental, and immunological factors result in the initiation and progress of AD (Novak and Bieber, 2005). Although many possible mechanisms of AD have been researched and proposed, its etiology remains unclear (Lee et al., 2010). In addition, despite the many studies on biological and pharmacological activities of BV and Mel, the therapeutic effects of BV and Mel against AD relevant mechanisms remain unknown. We found that BV and Mel possessed potent anti-atopic activities, as evidenced by improvements in the DNCB-induced AD-like skin lesions in animal models. *In vitro* studies using TNF-*α*/IFN-*γ*-stimulated human keratinocytes revealed that BV and Mel inhibited the exaggerated expression of chemokines, such as TARC/CCL17 and MDC/CCL22, and pro-inflammatory cytokines, including IL-1β, IL-6, and IFN-γ, through the blockade of the NF-κB and STAT signaling pathway. As a result, this study demonstrated that BV and Mel have immunomodulatory activity, and such activity was associated with the regulation of Th cell

This article is protected by copyright. All rights reserved.

differentiation, thereby ameliorating the inflammatory skin diseases caused by AD.

The Th cells are important components of immune cells to regulate the immune response to intracellular and extracellular pathogens by activating macrophages and cytotoxic T cells, releasing T-cell cytokines, and B-cell antibody class switching (Hahn and Erb, 1999). Mature Th cells are also known as $CD4^+$ T cells because they indicate the CD4 glycoprotein on their surface (Finlayson, 2012). These $CD4^+$ T cells play a key role in eliciting and maintaining AD inflammation. The differentiation of $CD4^+$ T cells leads to the generation of Th1 cells that secrete IFN-γ, Th2 cells that secrete IL-4, IL-5, and IL-13, or Th17 cells that secrete IL-17 and IL-22. Therefore, modulating T cell-elicited immune responses is a promising therapeutic approach for AD (Biedermann et al., 2015). In this study, we observed that DNCB induced the expression of IFN-γ and IL-4 via the activation of $CD4^+$ T cells. However, BV and Mel significantly suppressed both IFN-γ and IL-4 production by $CD4^+$ T cells.

Numerous studies have suggested that the cytokine TSLP acts as a master switch that triggers both the initiation and maintenance of AD (Ziegler et al., 2013). Besides, TSLP can act directly on naive $CD4^+$ T cells to promote cell proliferation and Th2 differentiation (Yao et al., 2013). TSLP was recently shown to be expressed in the epidermis after mechanical stimulation and play a principal role in the activation of Th2 cytokine-secreting invariant natural killer cells and serum IgE, which are increased in AD skin (Wu et al., 2010). IgE production is associated with a predominant Th2 cellular response. Our study showed that TSLP and IgE were increased in DNCB-induced AD-like mice, and BV and Mel decreased TSLP and IgE production. The inhibitory effects of BV and Mel on the expression of TSLP were confirmed by immunohistochemistry staining. In addition, multiple immune cells are activated by TSLP, including natural killer cells, dendritic cells, T cells, B cells, basophils, eosinophils, and mast cells, which promote allergic inflammation (Ziegler et al., 2013). In allergic inflammation, IgE is synthesized by B cells and induces the activation of mast cells, leading to the secretion of Th2 cytokines and histamine (Kim et al., 2012). In this study, we could observe the infiltration and degranulation of mast cells in DNCB-induced AD-like skin lesions. The topical application of BV and Mel to mice diminished DNCB-induced mast cell infiltration and degranulation.

This article is protected by copyright. All rights reserved.

Since Th1 and Th2 cell differentiation and their functions as well as keratinocyte activation are critical to AD development, an ideal therapeutic approach to AD may be a treatment with inhibitors that modulate T cell and keratinocyte activation and thus ameliorate AD symptoms. Keratinocytes play a critical role in atopic skin inflammation (Giustizieri et al., 2001). Many studies have shown that TARC/CCL17 and MDC/CCL22 play critical roles in the migration of lymphocytes to the skin; therefore, a decrease in the release of TARC/CCL17 and MDC/CCL22 in keratinocytes may be an effective target for the treatment of inflammatory skin diseases (Hatano et al., 2013). In this study, BV and Mel suppressed TNF-α/IFN-γ-induced TARC/CCL17, MDC/CCL22, IL-1β, and IL-6 expressions in HaCaT cells. The modulation of AD-associated chemokines and cytokines may yield therapeutic efficacy.

In addition, NF-κB is a crucial factor in the immune-inflammatory responses implicated in various skin diseases, including AD (Andrés et al., 2013). The activation of the NF-κB pathway leads to the transcription of numerous genes, including cytokines, chemokines, and growth factors that are involved in the initiation of the inflammatory response (Perera et al., 2012). The molecular mechanisms of BV and Mel on AD-related NF-κB and STAT pathways have not yet been fully delineated. Our findings show that BV and Mel inhibited the TNF-α/IFN-γ-stimulated NF-κB phosphorylation. In fact, the downregulation of this transcriptional factor may be the cause of the decrease of the cytokines measured in skin samples, as their transcription is dependent on NF-κB activation. The role of JAK/STAT signaling in AD was further evaluated in the present study.

JAK/STAT signaling pathways are key transcriptional mediators that are essential for various cell functions, and they are activated by several cytokines (Amano et al., 2015). Cytokine-mediated activation of STAT proteins plays an essential role in $CD4^+$ T cell differentiation and the regulation of immune responses (O'Shea et al., 2011). For example, STAT1 is induced by IFN-γ, IL-6, and epidermal growth factor; STAT2 is induced by IFN-α, STAT3 by epidermal growth factor and IL-6, and STAT4 by IL-12 (Shi et al., 2011). STAT3 is a main player in cutaneous inflammatory diseases, as well as in normal keratinocyte function. The increased phosphorylation of STAT3 has been observed in skin lesions where pro-inflammatory cytokines are involved (Andrés et al., 2013). BV and Mel prevented TNF-α/IFN-γ-stimulated JAK2 phosphorylation and the nuclear translocation of p-STAT1 and p-STAT3. NF-κB and JAK/STAT signaling pathways are involved in the regulation of TARC/CCL17 and MDC/CCL22 release in HaCaT cells. Thus, our results suggest that

This article is protected by copyright. All rights reserved.

suppressed activation of NF-κB and JAK/STAT signaling pathways by BV and Mel might decrease the production of chemokines and cytokines in keratinocytes and thus mitigate AD.

In summary, this study demonstrated the ameliorating effects of BV and Mel on the DNCB-induced AD-like skin lesions of Balb/c mice and TNF-α/IFN-γ-stimulated human keratinocyte HaCaT cells. BV and Mel reduced inflammatory symptoms in AD-like skin lesions by suppressing the production of Th1/Th2-associated and pro-inflammatory cytokines with a subsequent decrease of $CD4^+$ T cells, mast cell infiltration, and the release of serum IgE. In addition, BV and Mel improved the abnormal epidermal differentiation by restoring filaggrin expression. BV and Mel prevented the production of chemokines, most likely through the inhibition of NF-κB, STAT1, and STAT3 transcriptional activity in TNF-α/IFN-γ-stimulated keratinocytes. In conclusion, these results suggest that BV and Mel would be suitable for epicutaneous application, as topical administration is often applicable for the treatment of AD.

Author contributions

Hyun-Jin An and Kwan-Kyu Park designed the study and prepared the manuscript. Hyun-Jin An, Jung-Yeon Kim, Woon-Hae Kim, Mi-Gyeong Gwon, HyeMin Gu, MinJi Jeon, Sang-Mi Han, and InSook Park performed the overall experiments and analyzed the data. Sok Cheon Pak and Chong-Kee lee discussed the study. All authors have read and approved the final version of this manuscript.

Conflict of interest

The authors have no conflicts of interest

Accepted Article

This article is protected by copyright. All rights reserved.

Acknowledgments

This work was carried out with the support of "Cooperative Research Program for Agriculture Science & Technology Development (Project No. PJ01316601)" Rural Development Administration, Republic of Korea.

References

ALEXANDER, S. P., KELLY, E., MARRION, N. V., PETERS, J. A., FACCENDA, E., HARDING, S. D., PAWSON, A. J., SHARMAN, J. L., SOUTHAN, C., BUNEMAN, O. P., CIDLOWSKI, J. A., CHRISTOPOULOS, A., DAVENPORT, A. P., FABBRO, D., SPEDDING, M., STRIESSNIG, J. & DAVIES, J. A. 2017. THE CONCISE GUIDE TO PHARMACOLOGY 2017/18: Overview. *Br J Pharmacol,* 174 Suppl 1**,** S1-S16.

AMANO, W., NAKAJIMA, S., KUNUGI, H., NUMATA, Y., KITOH, A., EGAWA, G., DAINICHI, T., HONDA, T., OTSUKA, A., KIMOTO, Y., YAMAMOTO, Y., TANIMOTO, A., MATSUSHITA, M., MIYACHI, Y. & KABASHIMA, K. 2015. The Janus kinase inhibitor JTE-052 improves skin barrier function through suppressing signal transducer and activator of transcription 3 signaling. *J Allergy Clin Immunol,* 136**,** 667-677 e7.

AN, H. J., KIM, J. Y., KIM, W. H., HAN, S. M. & PARK, K. K. 2016. The Protective Effect of Melittin on Renal Fibrosis in an Animal Model of Unilateral Ureteral Obstruction. *Molecules,* 21.

ANDR S, R. M., MONTESINOS, M. C., NAVAL N, P., PAY , M. & TERENCIO, M. C. 2013. NF-κB and STAT3 inhibition as a therapeutic strategy in psoriasis: in vitro and in vivo effects of BTH. *Journal of Investigative Dermatology,* 133**,** 2362-2371.

BERKE, R., SINGH, A. & GURALNICK, M. 2012. Atopic dermatitis: an overview. *Am Fam Physician,* 86**,** 35-42.

BIEDERMANN, T., SKABYTSKA, Y., KAESLER, S. & VOLZ, T. 2015. Regulation of T Cell Immunity in Atopic Dermatitis by Microbes: The Yin and Yang of Cutaneous Inflammation. *Front Immunol,* 6**,** 353.

BLAKELY, K., GOODERHAM, M. & PAPP, K. 2016. Dupilumab, A Monoclonal Antibody for Atopic Dermatitis: A Review of Current Literature. *Skin Therapy Lett,* 21**,** 1-5.

BOGUNIEWICZ, M. & LEUNG, D. Y. 2011. Atopic dermatitis: a disease of altered skin barrier and immune dysregulation. *Immunol Rev,* 242**,** 233-46.

BRANDT, E. B. & SIVAPRASAD, U. 2011. Th2 Cytokines and Atopic Dermatitis. *J Clin Cell Immunol,* 2.

CHAN, C. C., LIOU, C. J., XU, P. Y., SHEN, J. J., KUO, M. L., LEN, W. B., CHANG, L. E. & HUANG, W. C. 2013. Effect of dehydroepiandrosterone on atopic dermatitis-like skin lesions induced by 1-chloro-2,4-dinitrobenzene in mouse. *J Dermatol Sci,* 72**,** 149-57.

This article is protected by copyright. All rights reserved.

Accepted Article

CHOI, J. K. & KIM, S. H. 2013. Rutin suppresses atopic dermatitis and allergic contact dermatitis. *Exp Biol Med (Maywood),* 238**,** 410-7.

CHOI, J. K., OH, H. M., LEE, S., PARK, J. W., KHANG, D., LEE, S. W., LEE, W. S., RHO, M. C. & KIM, S. H. 2013. Oleanolic acid acetate inhibits atopic dermatitis and allergic contact dermatitis in a murine model. *Toxicol Appl Pharmacol,* 269**,** 72-80.

COONDOO, A. 2012. The role of cytokines in the pathomechanism of cutaneous disorders. *Indian J Dermatol,* 57**,** 90-6.

DEL ROSSO, J. & FRIEDLANDER, S. F. 2005. Corticosteroids: options in the era of steroid-sparing therapy. *J Am Acad Dermatol,* 53**,** S50-8.

ELIAS, P. M. & SCHMUTH, M. 2009. Abnormal skin barrier in the etiopathogenesis of atopic dermatitis. *Curr Opin Allergy Clin Immunol,* 9**,** 437-46.

FINLAYSON, M. 2012. *Multiple sclerosis rehabilitation: From impairment to participation*, CRC Press.

FR HLICH, A., KISIELOW, J., SCHMITZ, I., FREIGANG, S., SHAMSHIEV, A. T., WEBER, J., MARSLAND, B. J., OXENIUS, A. & KOPF, M. 2009. IL-21R on T cells is critical for sustained functionality and control of chronic viral infection. *Science,* 324**,** 1576-1580.

GALLI, S. J. & TSAI, M. 2012. IgE and mast cells in allergic disease. *Nat Med,* 18**,** 693-704.

GIUSTIZIERI, M. L., MASCIA, F., FREZZOLINI, A., DE PIT , O., CHINNI, L. M., GIANNETTI, A., GIROLOMONI, G. & PASTORE, S. 2001. Keratinocytes from patients with atopic dermatitis and psoriasis show a distinct chemokine production profile in response to T cell–derived cytokines. *Journal of Allergy and Clinical Immunology,* 107**,** 871-877.

GUO, L., WEI, G., ZHU, J., LIAO, W., LEONARD, W. J., ZHAO, K. & PAUL, W. 2009. IL-1 family members and STAT activators induce cytokine production by Th2, Th17, and Th1 cells. *Proc Natl Acad Sci U S A,* 106**,** 13463-8.

HAHN, S. & ERB, P. 1999. The immunomodulatory role of CD4-positive cytotoxic T-lymphocytes in health and disease. *Int Rev Immunol,* 18**,** 449-64.

HATANO, Y., ADACHI, Y., ELIAS, P. M., CRUMRINE, D., SAKAI, T., KURAHASHI, R., KATAGIRI, K. & FUJIWARA, S. 2013. The Th2 cytokine, interleukin-4, abrogates the cohesion of normal stratum corneum in mice: implications for pathogenesis of atopic dermatitis. *Exp Dermatol,* 22**,** 30-5.

IRVINE, A. D., MCLEAN, W. H. & LEUNG, D. Y. 2011. Filaggrin mutations associated with skin and allergic diseases. *N Engl J Med,* 365**,** 1315-27.

JU, S. M., SONG, H. Y., LEE, S. J., SEO, W. Y., SIN, D. H., GOH, A. R., KANG, Y. H., KANG, I. J., WON, M. H., YI, J. S., KWON, D. J., BAE, Y. S., CHOI, S. Y. & PARK, J. 2009. Suppression of thymus- and activation-regulated chemokine (TARC/CCL17) production by 1,2,3,4,6-penta-O-galloyl-beta-D-glucose via blockade of NF-kappaB and STAT1 activation in the HaCaT cells. *Biochem Biophys Res Commun,* 387**,** 115-20.

JUNG, K. H., BAEK, H., KANG, M., KIM, N., LEE, S. Y. & BAE, H. 2017. Bee Venom Phospholipase A2 Ameliorates House Dust Mite Extract Induced Atopic Dermatitis Like Skin Lesions in Mice.

Accepted Article

This article is protected by copyright. All rights reserved.

Toxins (Basel), 9.

JUNG, M., CHOI, J., LEE, S. A., KIM, H., HWANG, J. & CHOI, E. H. 2014. Pyrrolidone carboxylic acid levels or caspase-14 expression in the corneocytes of lesional skin correlates with clinical severity, skin barrier function and lesional inflammation in atopic dermatitis. *J Dermatol Sci,* 76**,** 231-9.

JUNG, M. R., LEE, T. H., BANG, M. H., KIM, H., SON, Y., CHUNG, D. K. & KIM, J. 2012. Suppression of thymus- and activation-regulated chemokine (TARC/CCL17) production by 3-O-beta-D-glucopyanosylspinasterol via blocking NF-kappaB and STAT1 signaling pathways in TNF-alpha and IFN-gamma-induced HaCaT keratinocytes. *Biochem Biophys Res Commun,* 427**,** 236-41.

KALININ, A. E., KAJAVA, A. V. & STEINERT, P. M. 2002. Epithelial barrier function: assembly and structural features of the cornified cell envelope. *Bioessays,* 24**,** 789-800.

KAWASAKI, H., NAGAO, K., KUBO, A., HATA, T., SHIMIZU, A., MIZUNO, H., YAMADA, T. & AMAGAI, M. 2012. Altered stratum corneum barrier and enhanced percutaneous immune responses in filaggrin-null mice. *J Allergy Clin Immunol,* 129**,** 1538-46 e6.

KIDD, P. 2003. Th1/Th2 balance: the hypothesis, its limitations, and implications for health and disease. *Altern Med Rev,* 8**,** 223-46.

KIM, G. D., PARK, Y. S., AHN, H. J., CHO, J. J. & PARK, C. S. 2015. Aspartame Attenuates 2, 4-Dinitrofluorobenzene-Induced Atopic Dermatitis-Like Clinical Symptoms in NC/Nga Mice. *J Invest Dermatol,* 135**,** 2705-13.

KIM, T. H., KIM, G. D., JIN, Y. H., PARK, Y. S. & PARK, C. S. 2012. Omega-3 fatty acid-derived mediator, Resolvin E1, ameliorates 2,4-dinitrofluorobenzene-induced atopic dermatitis in NC/Nga mice. *Int Immunopharmacol,* 14**,** 384-91.

LARIVIERE, W. R. & MELZACK, R. 1996. The bee venom test: a new tonic-pain test. *Pain,* 66**,** 271-7.

LEE, G. & BAE, H. 2016. Bee Venom Phospholipase A2: Yesterday's Enemy Becomes Today's Friend. *Toxins (Basel),* 8**,** 48.

LEE, H. J. & LEE, S. H. 2014. Epidermal permeability barrier defects and barrier repair therapy in atopic dermatitis. *Allergy Asthma Immunol Res,* 6**,** 276-87.

LEE, K.-S., JEONG, E.-S., HEO, S.-H., SEO, J.-H., JEONG, D.-G. & CHOI, Y.-K. 2010. A novel model for human atopic dermatitis: application of repeated DNCB patch in BALB/c mice, in comparison with NC/Nga mice. *Laboratory Animal Research,* 26**,** 95-102.

LEE, K. H., CHO, K. A., KIM, J. Y., BAEK, J. H., WOO, S. Y. & KIM, J. W. 2011. Filaggrin knockdown and Toll-like receptor 3 (TLR3) stimulation enhanced the production of thymic stromal lymphopoietin (TSLP) from epidermal layers. *Exp Dermatol,* 20**,** 149-51.

LEE, W. R., KIM, K. H., AN, H. J., KIM, J. Y., CHANG, Y. C., CHUNG, H., PARK, Y. Y., LEE, M. L. & PARK, K. K. 2014. The protective effects of melittin on Propionibacterium acnes-induced inflammatory responses in vitro and in vivo. *J Invest Dermatol,* 134**,** 1922-30.

MCGRATH, J. C. & LILLEY, E. 2015. Implementing guidelines on reporting research using animals

This article is protected by copyright. All rights reserved.

(ARRIVE etc.): new requirements for publication in BJP. *Br J Pharmacol,* 172**,** 3189-3193.

MISERY, L. 2011. Therapeutic perspectives in atopic dermatitis. *Clin Rev Allergy Immunol,* 41**,** 267-71.

MIZUTANI, N., SAE-WONG, C., KANGSANANT, S., NABE, T. & YOSHINO, S. 2015. Thymic stromal lymphopoietin-induced interleukin-17A is involved in the development of IgE-mediated atopic dermatitis-like skin lesions in mice. *Immunology,* 146**,** 568-81.

NAIR, M. & PEATE, I. 2015. *Pathophysiology for Nurses at a Glance*, John Wiley & Sons.

NOVAK, N. & BIEBER, T. 2005. The role of dendritic cell subtypes in the pathophysiology of atopic dermatitis. *J Am Acad Dermatol,* 53**,** S171-S176.

O'SHEA, J. J., LAHESMAA, R., VAHEDI, G., LAURENCE, A. & KANNO, Y. 2011. Genomic views of STAT function in CD4+ T helper cell differentiation. *Nat Rev Immunol,* 11**,** 239-50.

OYOSHI, M. K., HE, R., KUMAR, L., YOON, J. & GEHA, R. S. 2009. Cellular and molecular mechanisms in atopic dermatitis. *Adv Immunol,* 102**,** 135-226.

PARK, K. D., PAK, S. C. & PARK, K. K. 2016. The Pathogenetic Effect of Natural and Bacterial Toxins on Atopic Dermatitis. *Toxins (Basel),* 9.

PERERA, G. K., DI MEGLIO, P. & NESTLE, F. O. 2012. Psoriasis. *Annu Rev Pathol,* 7**,** 385-422.

QI, X. F., KIM, D. H., YOON, Y. S., LI, J. H., SONG, S. B., JIN, D., HUANG, X. Z., TENG, Y. C. & LEE, K. J. 2009. The adenylyl cyclase-cAMP system suppresses TARC/CCL17 and MDC/CCL22 production through p38 MAPK and NF-kappaB in HaCaT keratinocytes. *Mol Immunol,* 46**,** 1925-34.

QI, X. F., KIM, D. H., YOON, Y. S., SONG, S. B., TENG, Y. C., CAI, D. Q. & LEE, K. J. 2012. Bambusae caulis in Liquamen Suppresses the Expression of Thymus and Activation-Regulated Chemokine and Macrophage-Derived Chemokine in Human Keratinocytes due to Antioxidant Effect. *Evid Based Complement Alternat Med,* 2012**,** 617494.

RAGHURAMAN, H. & CHATTOPADHYAY, A. 2007. Melittin: a membrane-active peptide with diverse functions. *Biosci Rep,* 27**,** 189-223.

SHAH, P. P., DESAI, P. R. & SINGH, M. 2012. Effect of oleic acid modified polymeric bilayered nanoparticles on percutaneous delivery of spantide II and ketoprofen. *J Control Release,* 158**,** 336-45.

SHI, X., JIN, L., DANG, E., CHANG, T., FENG, Z., LIU, Y. & WANG, G. 2011. IL-17A upregulates keratin 17 expression in keratinocytes through STAT1- and STAT3-dependent mechanisms. *J Invest Dermatol,* 131**,** 2401-8.

SOHN, E. H., JANG, S. A., LEE, C. H., JANG, K. H., KANG, S. C., PARK, H. J. & PYO, S. 2011. Effects of korean red ginseng extract for the treatment of atopic dermatitis-like skin lesions in mice. *J Ginseng Res,* 35**,** 479-86.

SON, D. J., LEE, J. W., LEE, Y. H., SONG, H. S., LEE, C. K. & HONG, J. T. 2007. Therapeutic application of anti-arthritis, pain-releasing, and anti-cancer effects of bee venom and its constituent compounds. *Pharmacol Ther,* 115**,** 246-70.

This article is protected by copyright. All rights reserved.

SOUTHAN, C., SHARMAN, J. L., BENSON, H. E., FACCENDA, E., PAWSON, A. J., ALEXANDER, S. P., BUNEMAN, O. P., DAVENPORT, A. P., MCGRATH, J. C., PETERS, J. A., SPEDDING, M., CATTERALL, W. A., FABBRO, D. & DAVIES, J. A. 2016. The IUPHAR/BPS Guide to PHARMACOLOGY in 2016: towards curated quantitative interactions between 1300 protein targets and 6000 ligands. *Nucleic Acids Res,* 44**,** D1054-68.

SUGIURA, K., SHAMOTO, M., SAKAMOTO, N., SHINZATO, M., OSADA, A., SUGIURA, M., HAYAKAWA, R. & KATO, Y. 2003. It is true that, when Langerhans cells migrate from the skin to the lymph node, they are transported via lymph vessels. *Dermatology,* 206**,** 222-224.

TAN, R. A. & CORREN, J. 2011. The relationship of rhinitis and asthma, sinusitis, food allergy, and eczema. *Immunol Allergy Clin North Am,* 31**,** 481-91.

WU, W. H., PARK, C. O., OH, S. H., KIM, H. J., KWON, Y. S., BAE, B. G., NOH, J. Y. & LEE, K. H. 2010. Thymic stromal lymphopoietin-activated invariant natural killer T cells trigger an innate allergic immune response in atopic dermatitis. *J Allergy Clin Immunol,* 126**,** 290-9, 299 e1-4.

YAO, W., ZHANG, Y., JABEEN, R., NGUYEN, E. T., WILKES, D. S., TEPPER, R. S., KAPLAN, M. H. & ZHOU, B. 2013. Interleukin-9 is required for allergic airway inflammation mediated by the cytokine TSLP. *Immunity,* 38**,** 360-372.

ZIEGLER, S. F., ROAN, F., BELL, B. D., STOKLASEK, T. A., KITAJIMA, M. & HAN, H. 2013. The biology of thymic stromal lymphopoietin (TSLP). *Adv Pharmacol,* 66**,** 129-55.

Accepted Article

This article is protected by copyright. All rights reserved.

Figures and figure legends

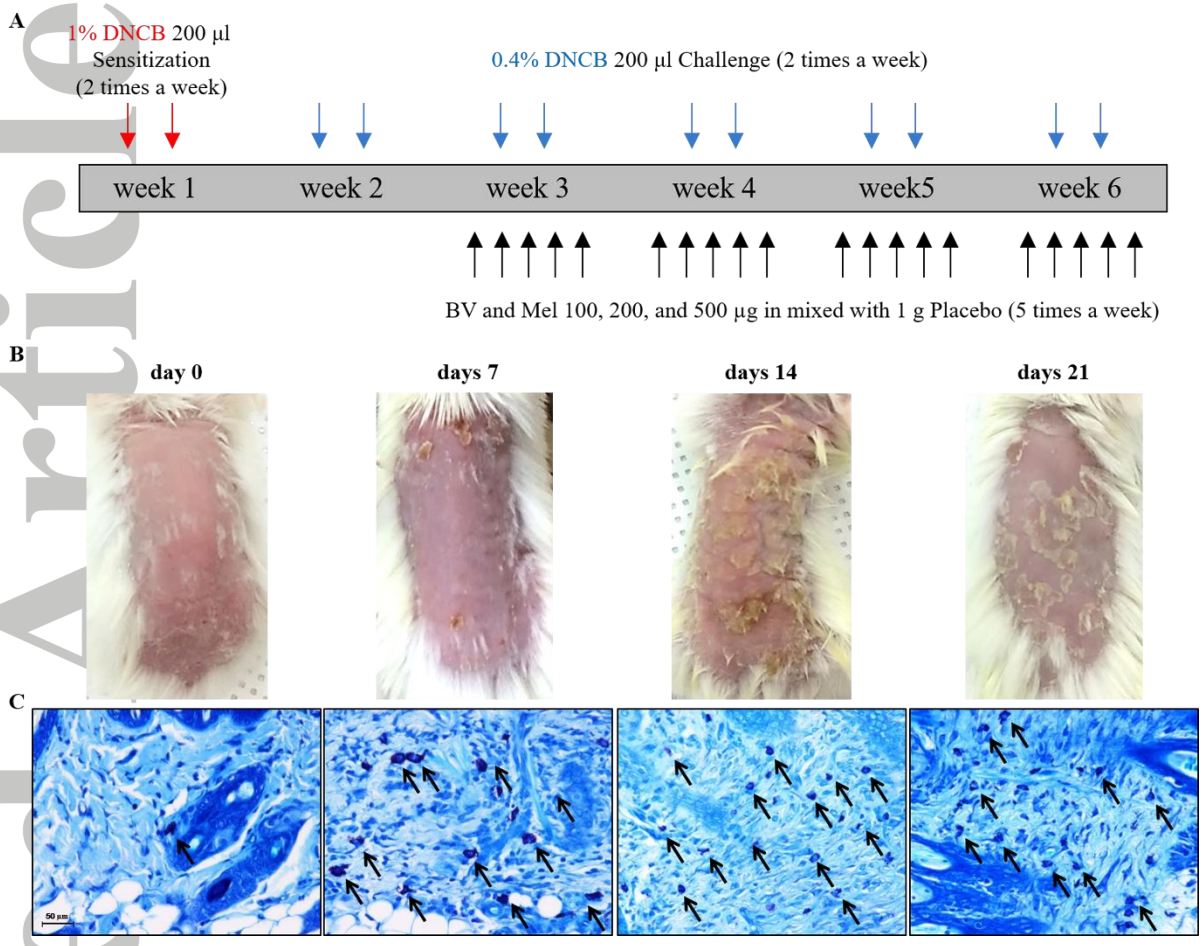


Figure 1. 1-chloro-2,4-dinitrobenzene (DNCB)-induced atopic dermatitis (AD)-like symptoms in Balb/c mice. (A) Schematic depiction of the experimental procedure. (B) Representative clinical features and (C) corresponding histopathological analysis of mouse dorsal skin are shown. The representative mast cells infiltrations were indicated by arrows. Scale bar = 50 µm.

Accepted Article

This article is protected by copyright. All rights reserved.

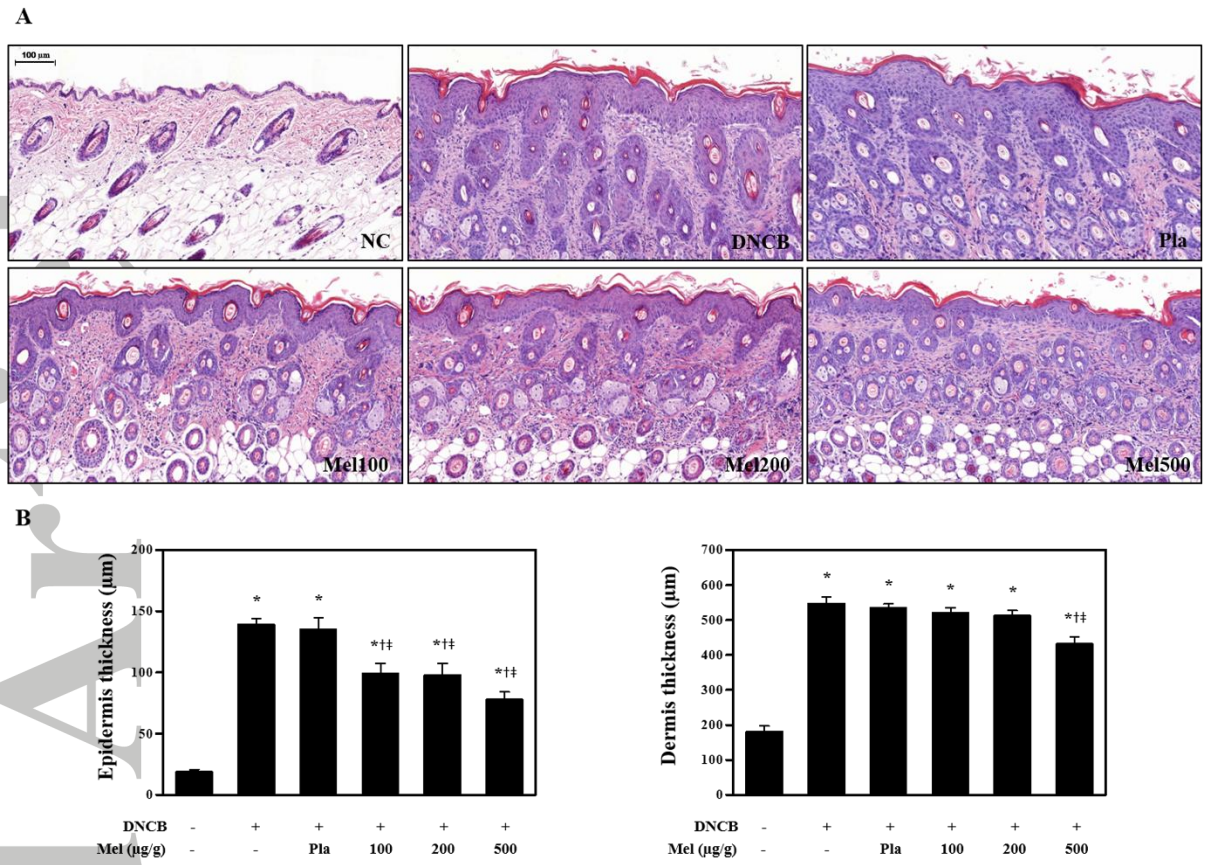


Figure 2. Effects of Mel on DNCB-induced changes in (A) epidermal hyperplasia and a heavy dermal cell infiltration and (B) epidermal thickness and dermal thickness (n = 5). Scale bar = 100 μm. *$p < 0.05$ *vs.* NC; $^{+}p < 0.05$ *vs.* DNCB; ǂ$p < 0.05$ *vs.* Pla; NC: normal control; DNCB: DNCB-sensitized and challenged; Pla: placebo; Mel 100: Mel 100 μg; Mel 200: Mel 200 μg; Mel 500: Mel 500 μg.

Accepted Article

This article is protected by copyright. All rights reserved.

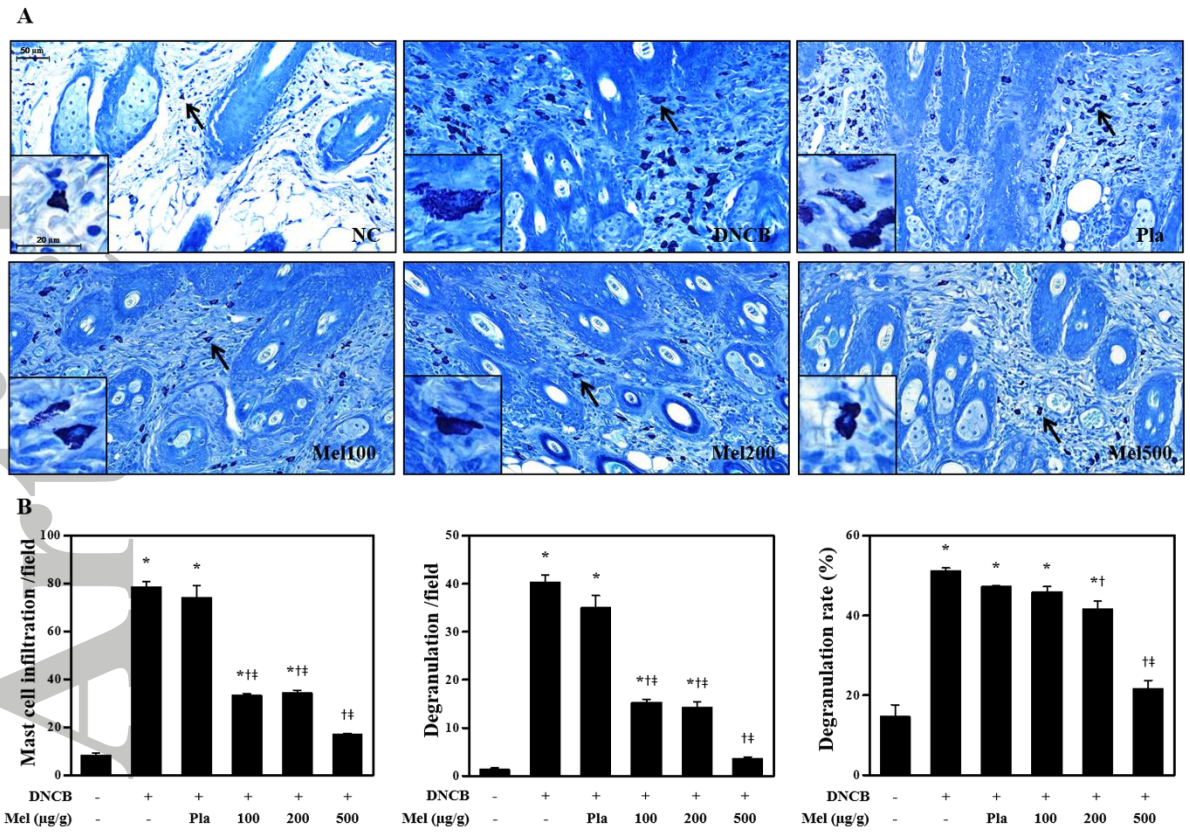


Figure 3. Effects of Mel on DNCB-induced changes in mast cell infiltration and degranulation. The representative mast cells were indicated by arrows (A). (B) The number of mast cells and degranulated mast cells were counted from all fields per section (n = 5). Scale bar = 50 μm. The enlarged frames scale bar = 20 μm. *$p < 0.05$ vs. NC; $^{+}p < 0.05$ vs. DNCB; $^{‡}p < 0.05$ vs. Pla; NC: normal control; DNCB: DNCB-sensitized and challenged; Pla: placebo; Mel100: Mel 100 μg; Mel200: Mel 200 μg; Mel500: Mel 500 μg.

Accepted Article

This article is protected by copyright. All rights reserved.

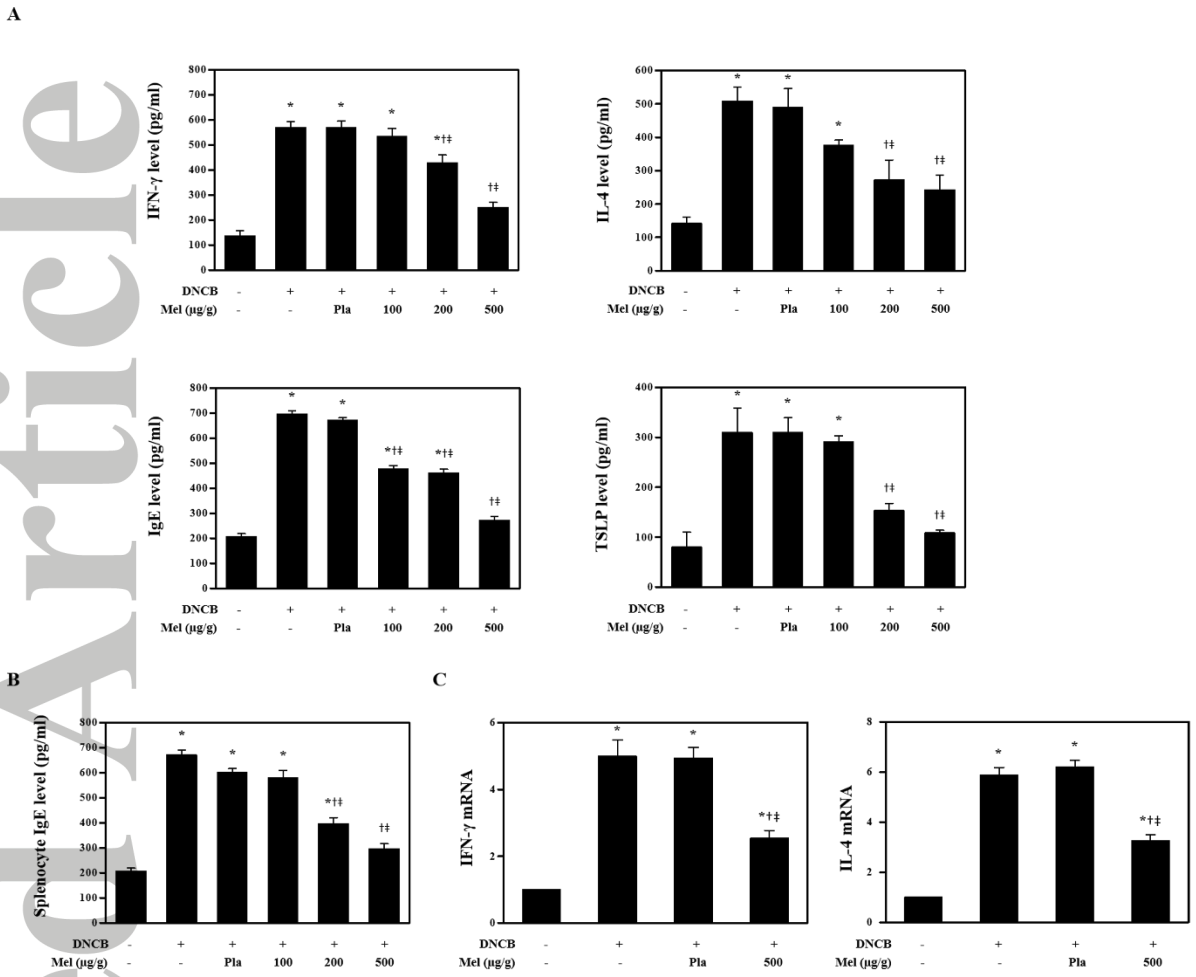


Figure 4. Effects of Mel on DNCB-induced changes in the serum levels of IFN-γ, IL-4, IgE, and TSLP, which were determined by ELISA kits (n = 5) (A). (B) Effects of Mel on DNCB-induced IgE in splenocytes of Balb/c. The IgE level in cultured splenocytes was measured by ELISA (n = 5). (C) Real-time PCR analyses show that Mel treatment inhibited the mRNA levels of IFN-γ and IL-4 (n = 5). *$p < 0.05$ *vs.* NC; $^{+}p < 0.05$ *vs.* DNCB; ǂ$p < 0.05$ *vs.* Pla; NC: normal control; DNCB: DNCB-sensitized and challenged; Pla: placebo; Mel100: Mel 100 μg; Mel200: Mel 200 μg; Mel500: Mel 500 μg.

Accepted Article

This article is protected by copyright. All rights reserved.

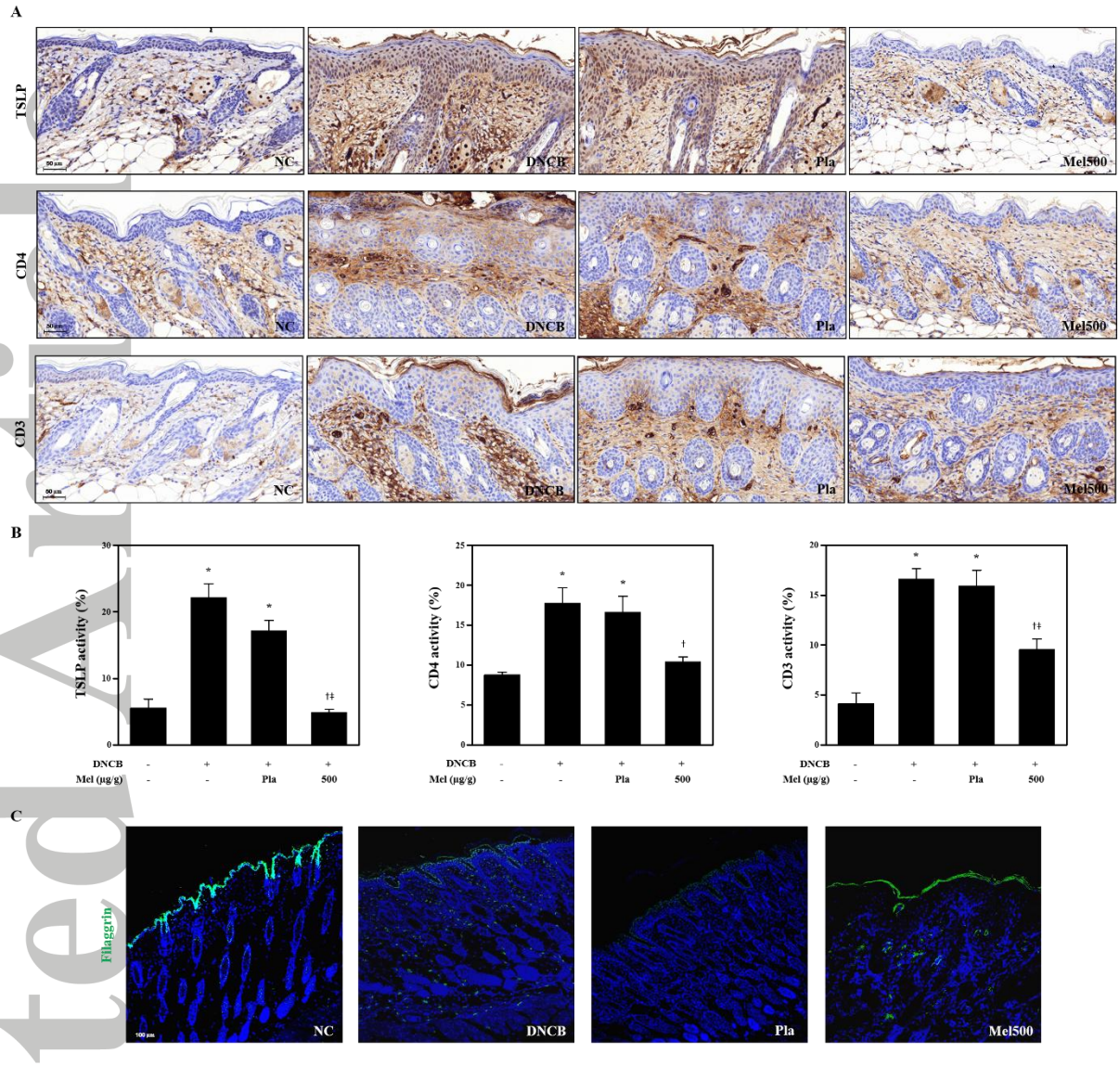


Figure 5. Effects of Mel on TSLP expression, $CD4^+$ and $CD3^+$ T cells in DNCB-sensitized mice. (A) Histological images and (B) graphs indicating the relative percentage of TSLP expression and $CD4^+$ and $CD3^+$ immunopositive cells of the dorsal skin sections (n = 5). (C) Effects of Mel on abnormal epidermal differentiation. Immunofluorescence staining of sections of skin with antibody specific for filaggrin shows the expression of epidermal differentiation markers as labeled with FITC, green. Cells were counterstained with Hoechst 33342 (blue). Scale bar = 100 μm. *$p < 0.05$ vs. NC; $^+p < 0.05$ vs. DNCB; ǂ$p < 0.05$ vs. Pla; NC: normal control; DNCB: DNCB-sensitized and challenged; Pla: placebo; Mel500: Mel 500 μg.

This article is protected by copyright. All rights reserved.

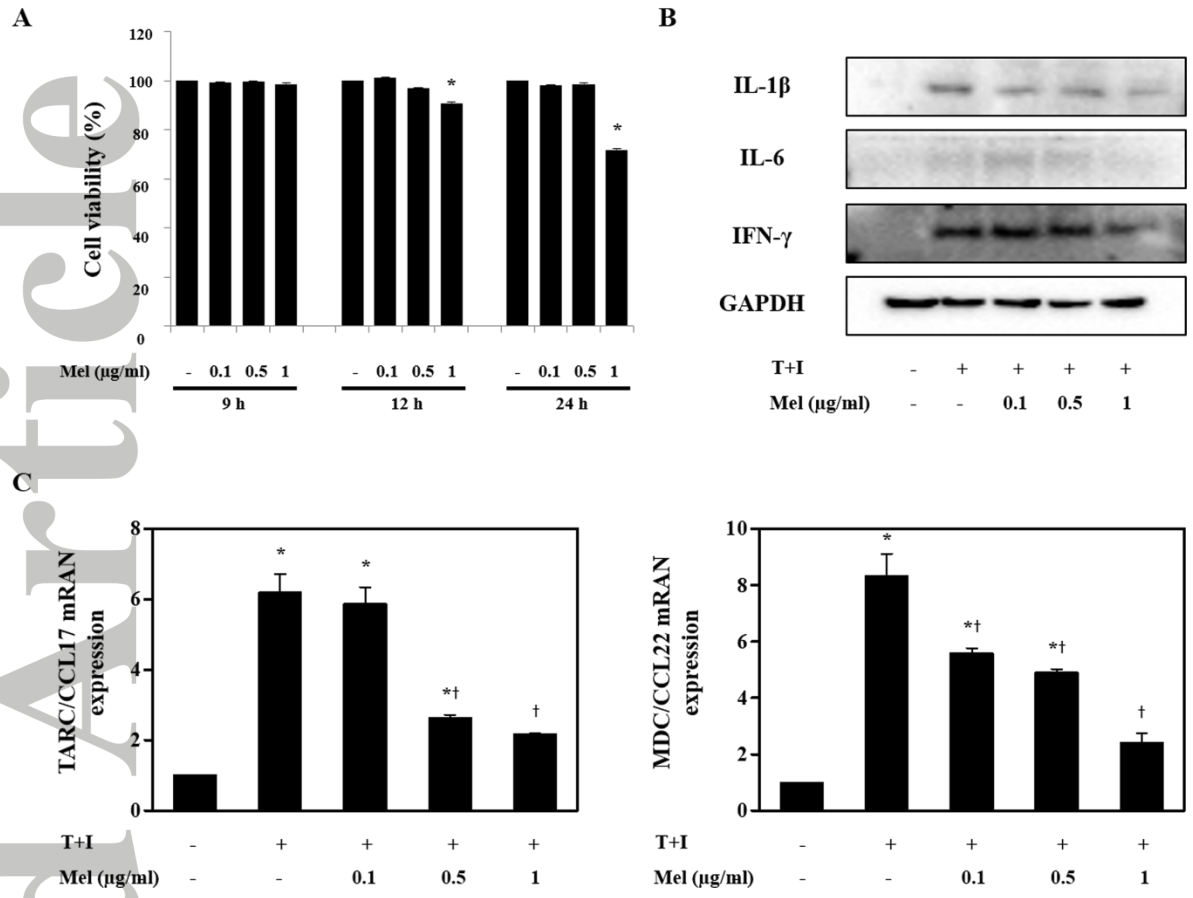


Figure 6. Cytotoxic effects of (A) Mel on HaCaT cells. Cell viability was determined by CCK-8 assay (n = 5). Effects of Mel on the chemokine expressions of cytokines (B) and chemokines (n = 5) (C) in HaCaT cells that were stimulated by TNF-α/IFN-γ. T+I: TNF-α/IFN-γ-stimulated; *$p < 0.05$ vs. no treatment. $^{+}p < 0.05$ vs. TNF-α/IFN-γ alone.

Accepted Article

This article is protected by copyright. All rights reserved.

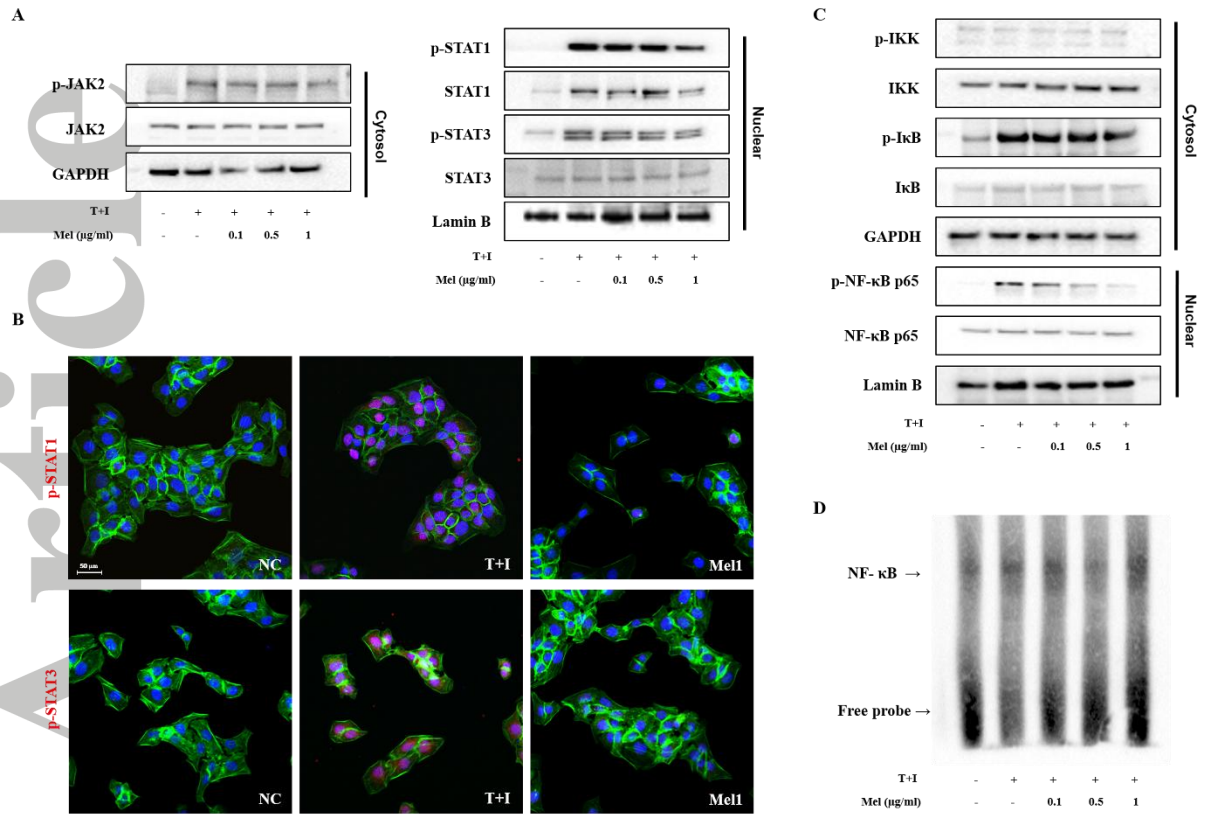
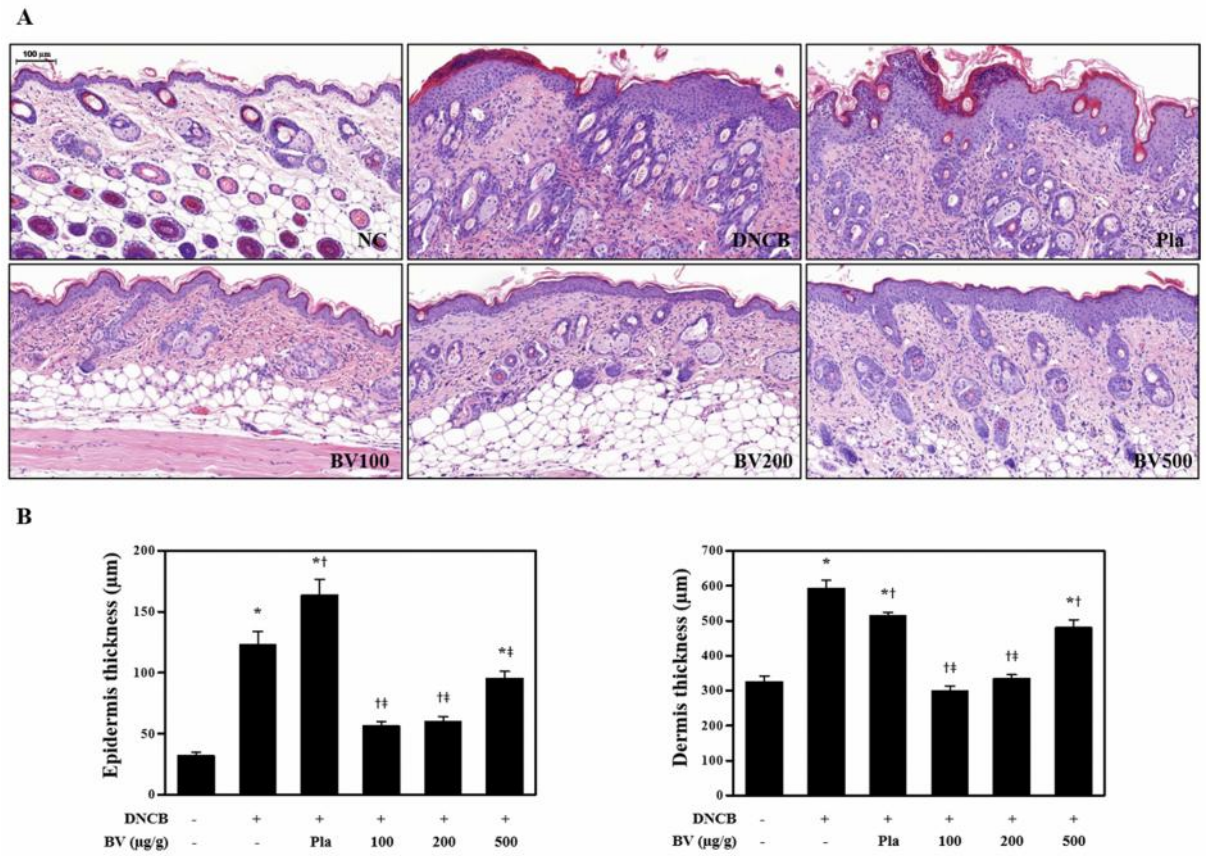


Figure 7. Effects of Mel on activation of the (A) JAK2, STAT1, and STAT3 signaling pathways in TNF-α/IFN-γ-stimulated HaCaT cells. (B) Immunofluorescence staining for p-STAT1 and p-STAT3 (labeled with Alexa Fluor 555, red), and F-actin (labeled with Alexa Fluor 488, green). Cells were counterstained with Hoechst 33342 (blue). Effects of Mel on activation of the (C) NF-κB signaling pathway in TNF-α/IFN-γ-stimulated HaCaT cells. (D) NF-κB DNA binding activity in the nuclear extract was measured by EMSA. Representative images from each group. Scale bar = 50 μm. NC: normal control; T+I: TNF-α/IFN-γ-stimulated; Mel1: TNF-α/IFN-γ-stimulated + 1 μg/ml Mel.

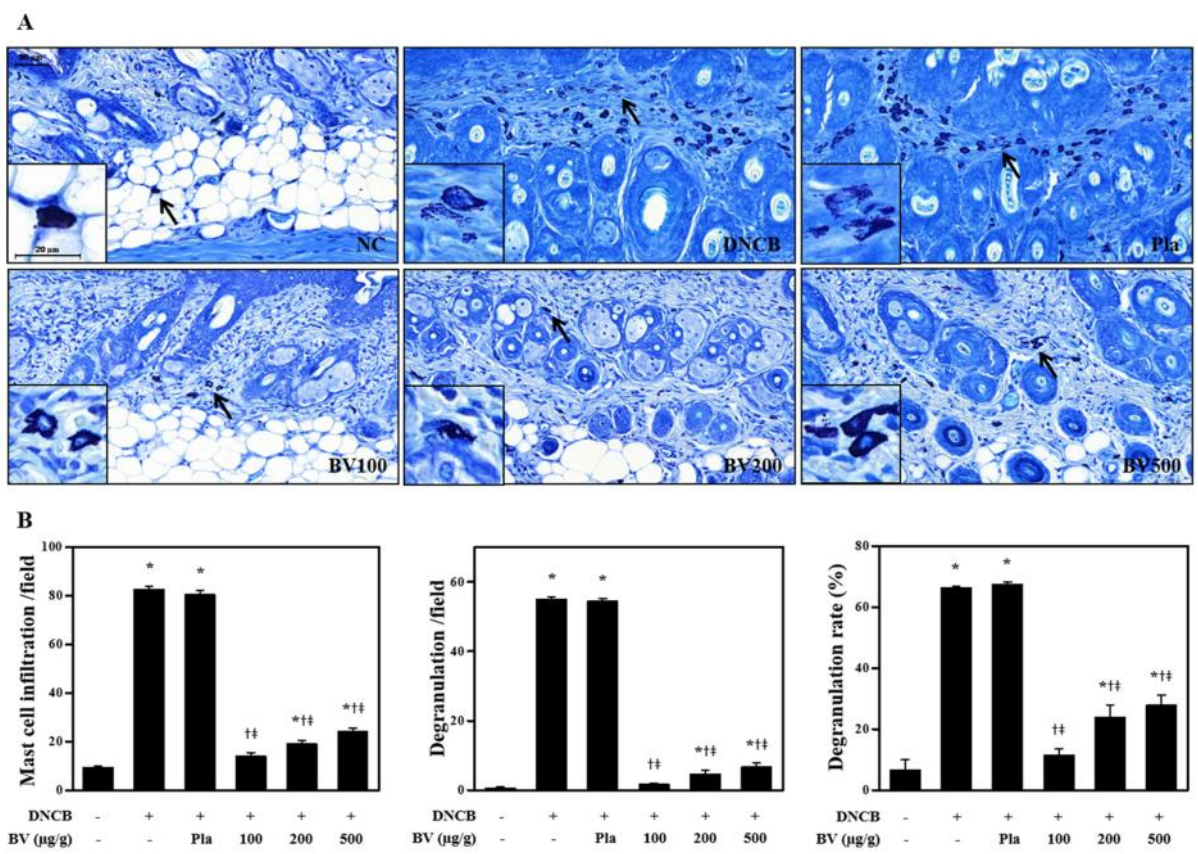
Accepted Article

This article is protected by copyright. All rights reserved.

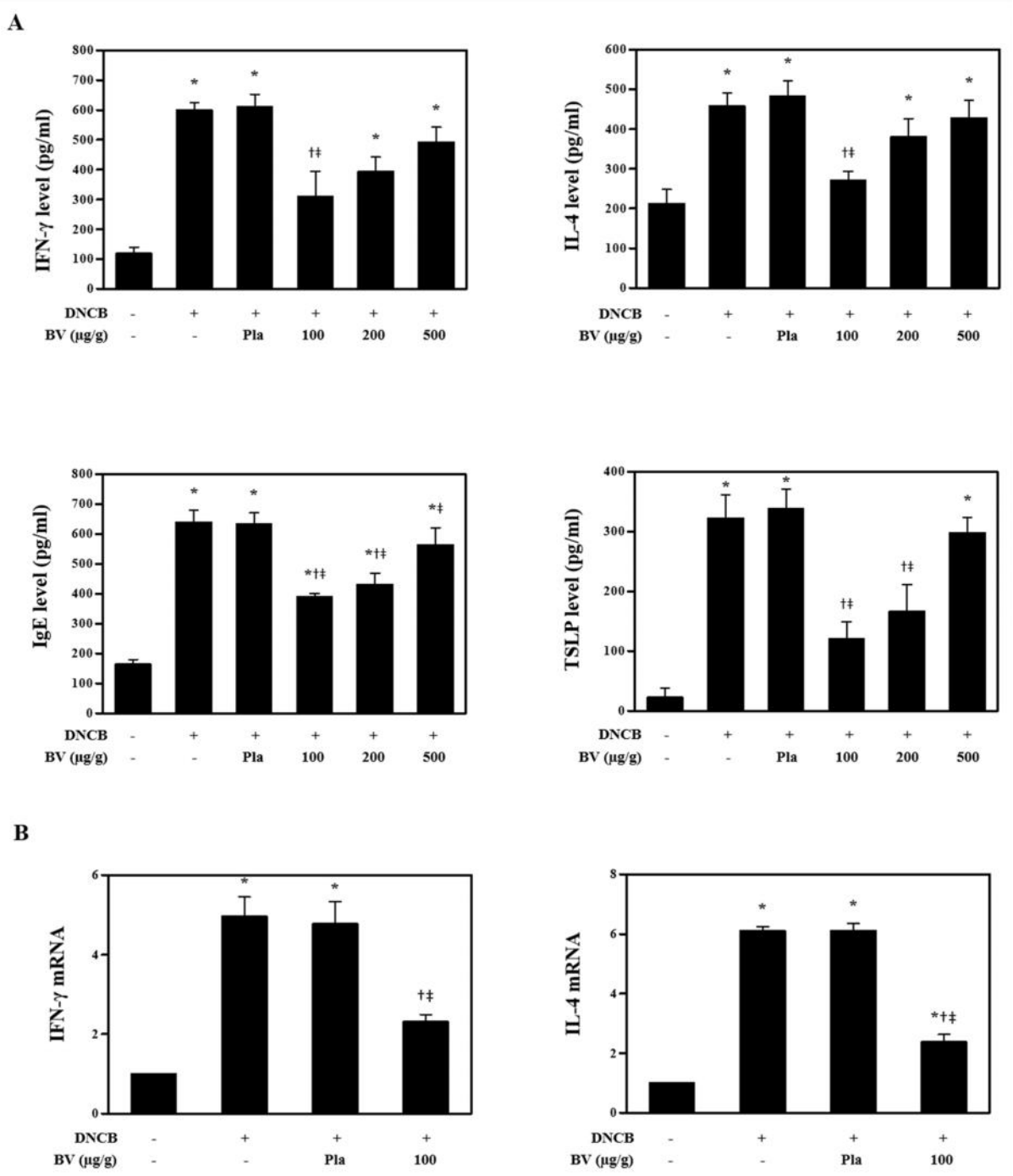
Supplementary figures and figure legends



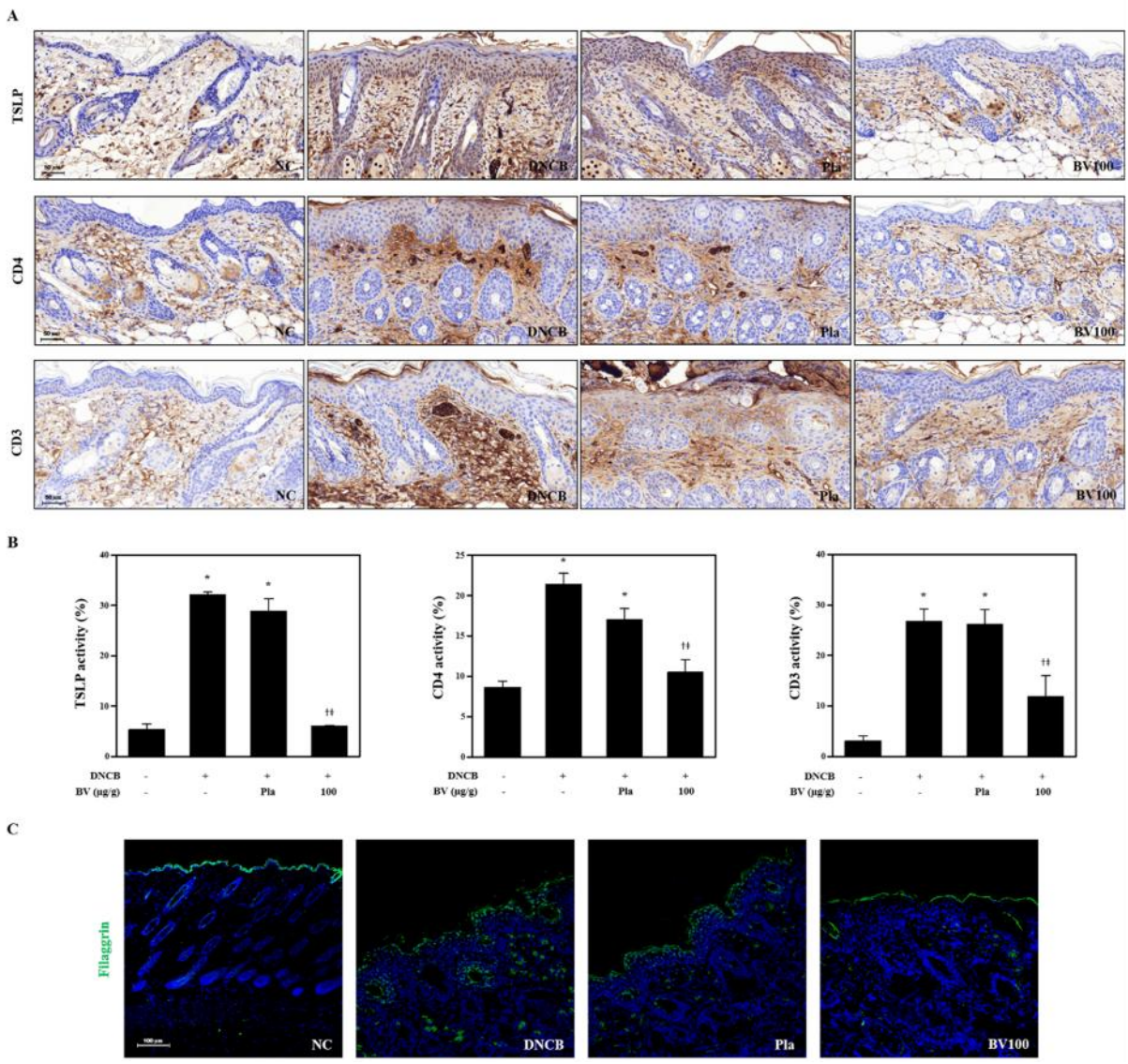
Supplementary figure S1. Effects of BV on DNCB-induced changes in (A) epidermal hyperplasia and a heavy dermal cell infiltration and (B) epidermal thickness and dermal thickness (n = 5). Scale bar = 100 μm. *p < 0.05 *vs.* NC; ^{+}p < 0.05 *vs.* DNCB; ǂp < 0.05 *vs.* Pla; NC: normal control; DNCB: DNCB-sensitized and challenged; Pla: placebo; BV100: BV 100 μg; BV200: BV 200 μg; BV500: BV 500 μg.



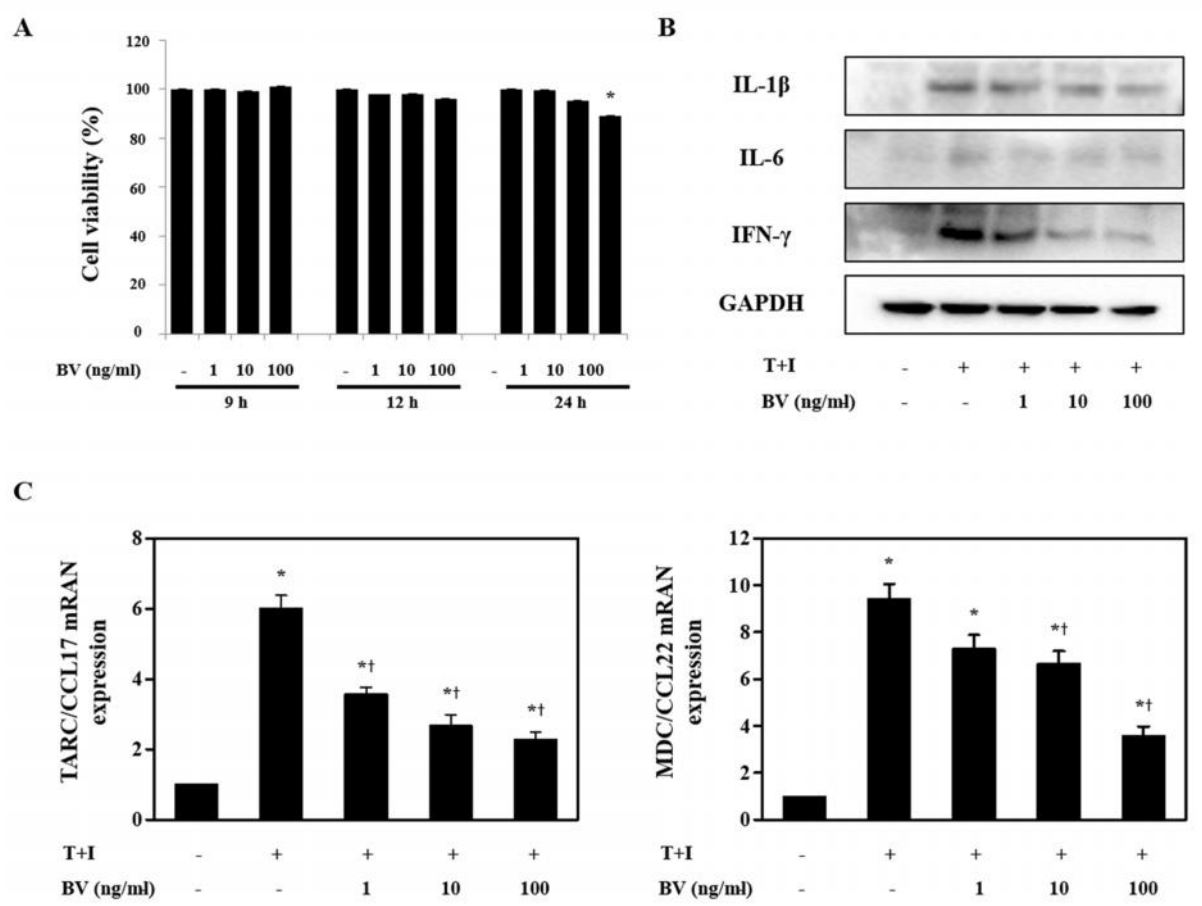
Supplementary figure S2. Effects of BV on DNCB-induced changes in mast cell infiltration and degranulation. The representative mast cells were indicated by arrows (A). (B) The number of mast cells and degranulated mast cells were counted from all fields per section (n = 5). Scale bar = 50 μm. The enlarged frames scale bar = 20 μm. *$p < 0.05$ *vs.* NC; $^{+}p < 0.05$ *vs.* DNCB; ǂ$p < 0.05$ *vs.* Pla; NC: normal control; DNCB: DNCB-sensitized and challenged; Pla: placebo; BV100: BV 100 μg; BV200: BV 200 μg; BV500: BV 500 μg.



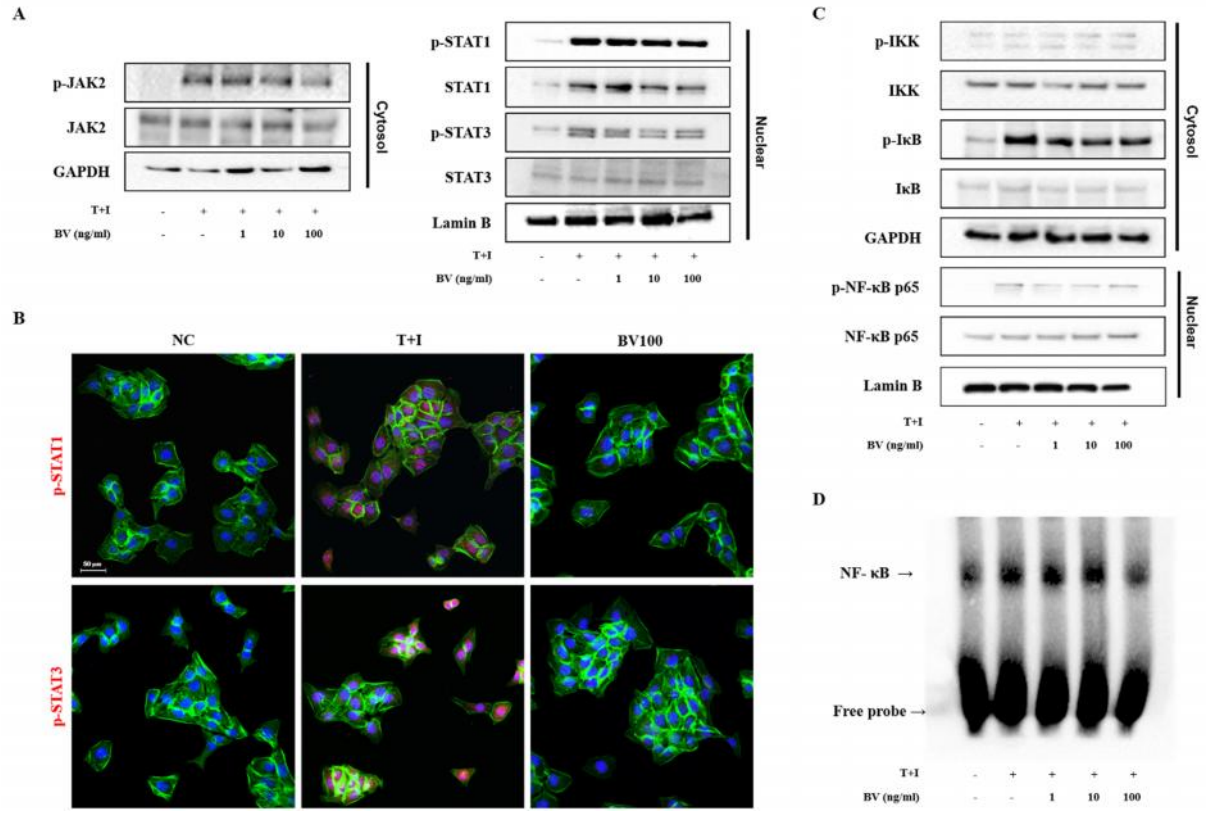
Supplementary figure S3. Effects of BV on DNCB-induced changes in the serum levels of IFN-γ, IL-4, IgE, and TSLP, which were determined by ELISA kits (n = 5) (A). (B) Real-time PCR analyses show that BV treatment inhibited the mRNA levels of IFN-γ and IL-4 (n = 5). *p < 0.05 *vs.* NC; ^{+}p < 0.05 *vs.* DNCB; ǂp < 0.05 *vs.* Pla; NC: normal control; DNCB: DNCB-sensitized and challenged; Pla: placebo; BV100: BV 100 μg; BV200: BV 200 μg; BV500: BV 500 μg.



Supplementary figure S4. Effects of BV on TSLP expression, $CD4^+$ and $CD3^+$ T cells in DNCB-sensitized mice. (A) Histological images and (B) graphs indicating the relative percentage of TSLP expression and $CD4^+$ and CD 3^+ immunopositive cells of the dorsal skin sections (n = 5). (C) Effects of BV on abnormal epidermal differentiation. Immunofluorescence staining of sections of skin with antibody specific for filaggrin shows the expression of epidermal differentiation markers as labeled with FITC, green. Cells were counterstained with Hoechst 33342 (blue). Scale bar = 100 μm. *$p < 0.05$ *vs.* NC; $^+p < 0.05$ *vs.* DNCB; ǂ$p < 0.05$ *vs.* Pla; NC: normal control; DNCB: DNCB-sensitized and challenged; Pla: placebo; BV100: BV 100 μg.

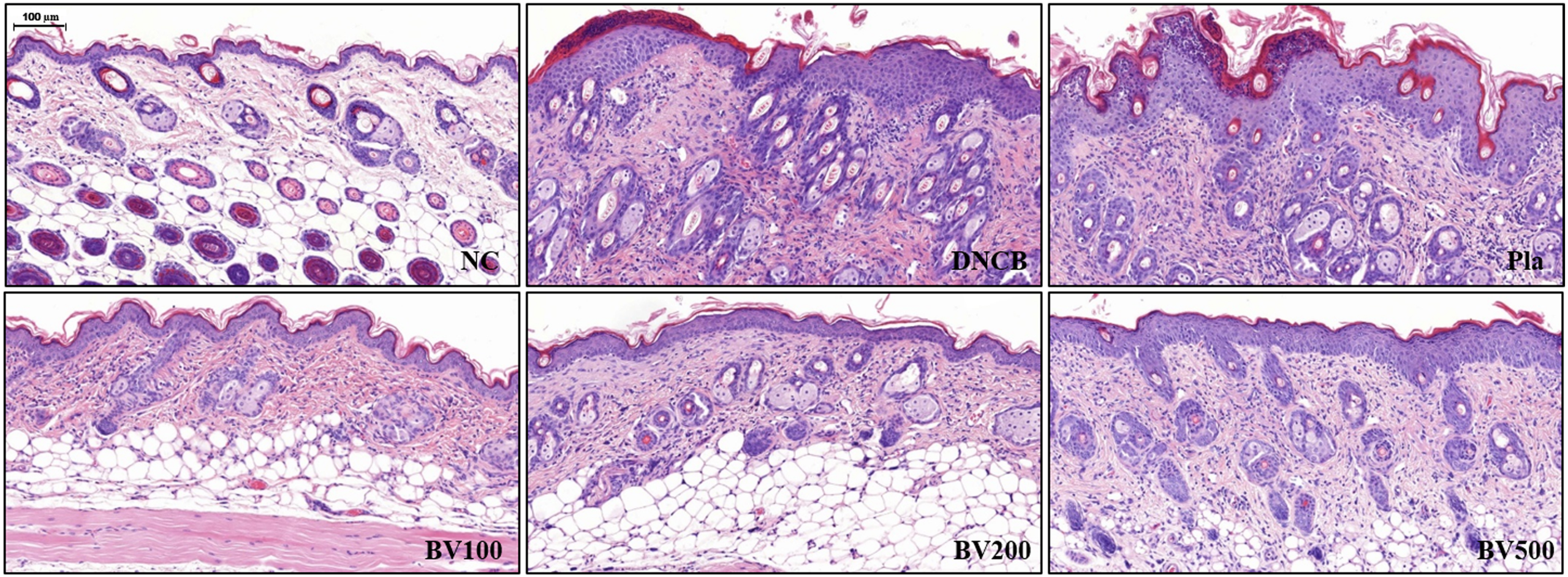


Supplementary figure S5. Cytotoxic effects of (A) BV on HaCaT cells. Cell viability was determined by CCK-8 assay ($n = 5$). Effects of BV on the chemokine expressions of cytokines (B) and chemokines ($n = 5$) (C) in HaCaT cells that were stimulated by TNF-α/IFN-γ. T+I: TNF-α/IFN-γ-stimulated; *$p < 0.05$ vs. no treatment. $^{+}p < 0.05$ vs. TNF-α/IFN-γ alone.

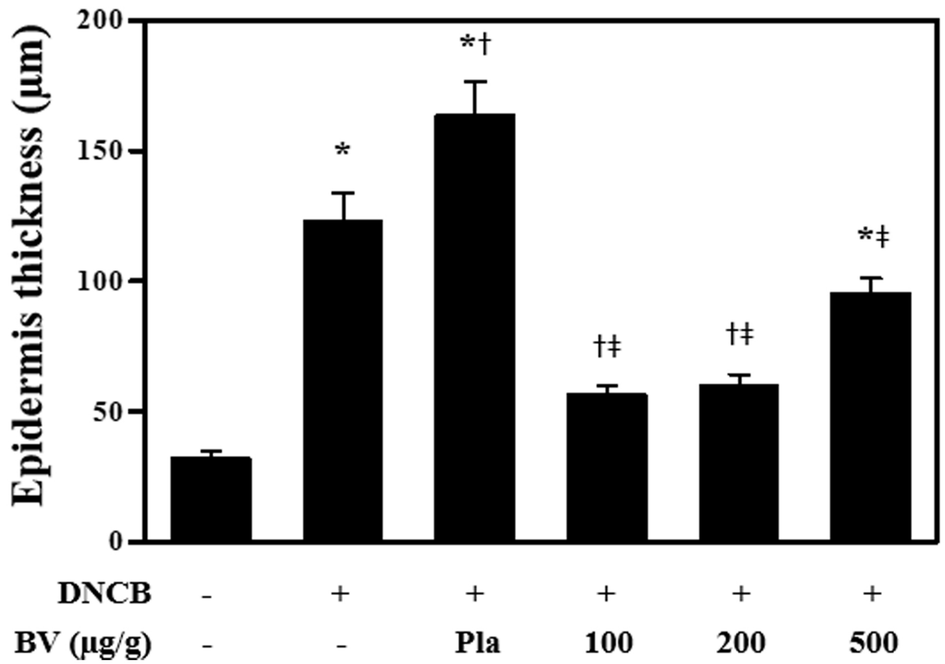


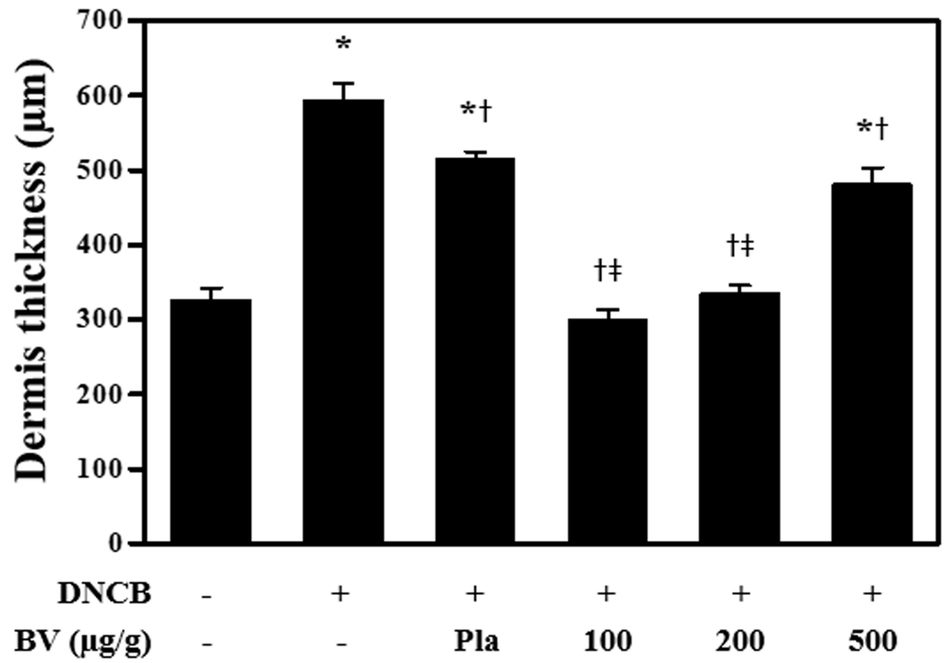
Supplementary figure S6. Effects of BV on activation of the (A) JAK2, STAT1, and STAT3 signaling pathway in TNF-α/IFN-γ-stimulated HaCaT cells. (B) Immunofluorescence staining for p-STAT1 and p-STAT3 (labeled with Alexa Fluor 555, red), and F-actin (labeled with Alexa Fluor 488, green). Cells were counterstained with Hoechst 33342 (blue). Effects of BV on activation of the (C) NF-κB signaling pathway in TNF-α/IFN-γ-stimulated HaCaT cells. (D) NF-κB DNA binding activity in the nuclear extract was measured by EMSA. Representative images from each group. Scale bar = 50 μm. NC: normal control; T+I: TNF-α/IFN-γ-stimulated; Mel1: TNF-α/IFN-γ-stimulated + 100 ng/ml BV.

A

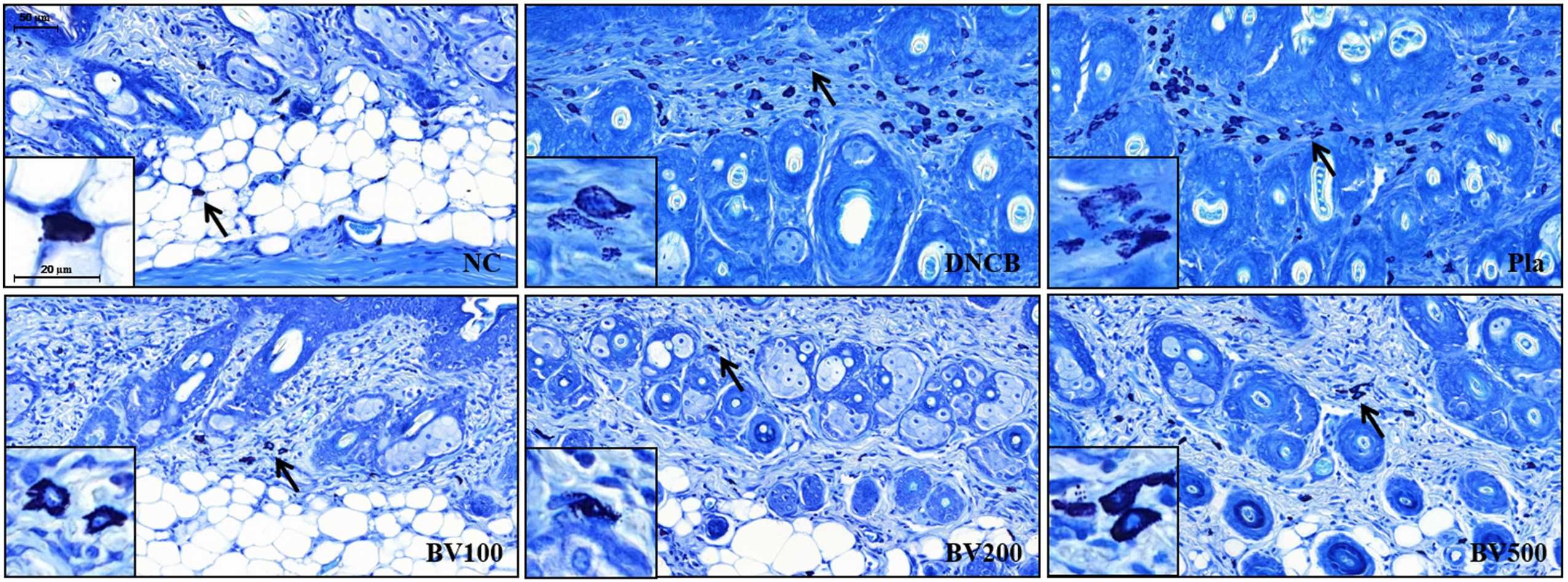

100 μm
NC
DNCB
Pla
BV100
BV200
BV500

B

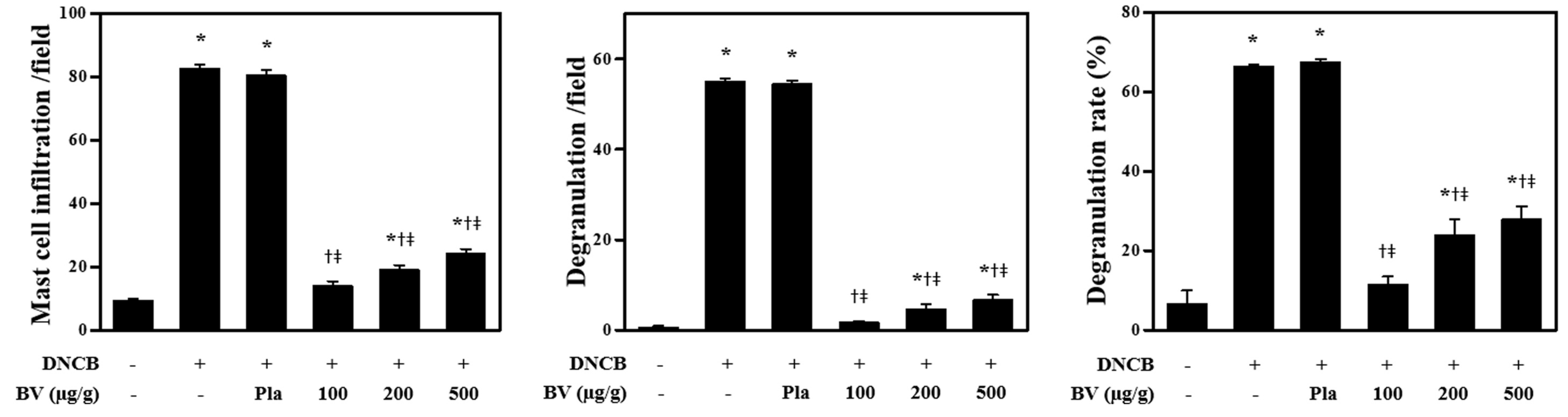

Epidermis thickness (μm)
200
150
100
50
0
*
*†
†‡
†‡
*‡
DNCB - + + + + +
BV (μg/g) - - Pla 100 200 500


Dermis thickness (μm)
700
600
500
400
300
200
100
0
*
*†
†‡
†‡
*†
DNCB - + + + + +
BV (μg/g) - - Pla 100 200 500

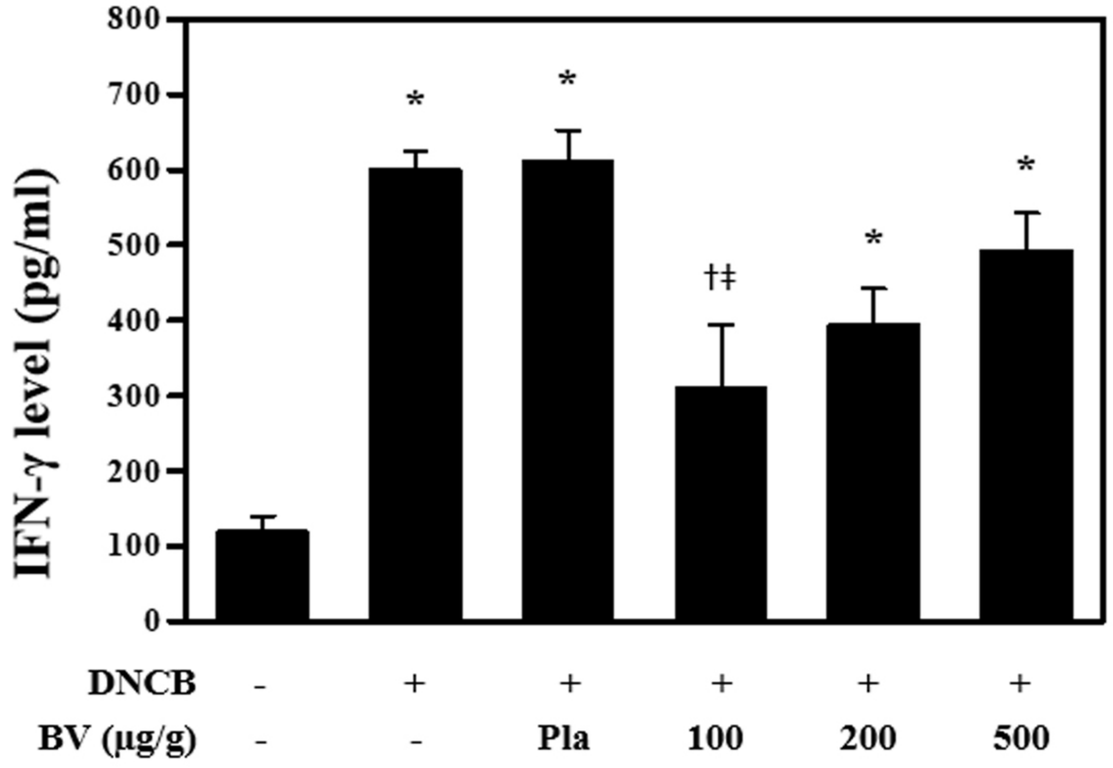
A

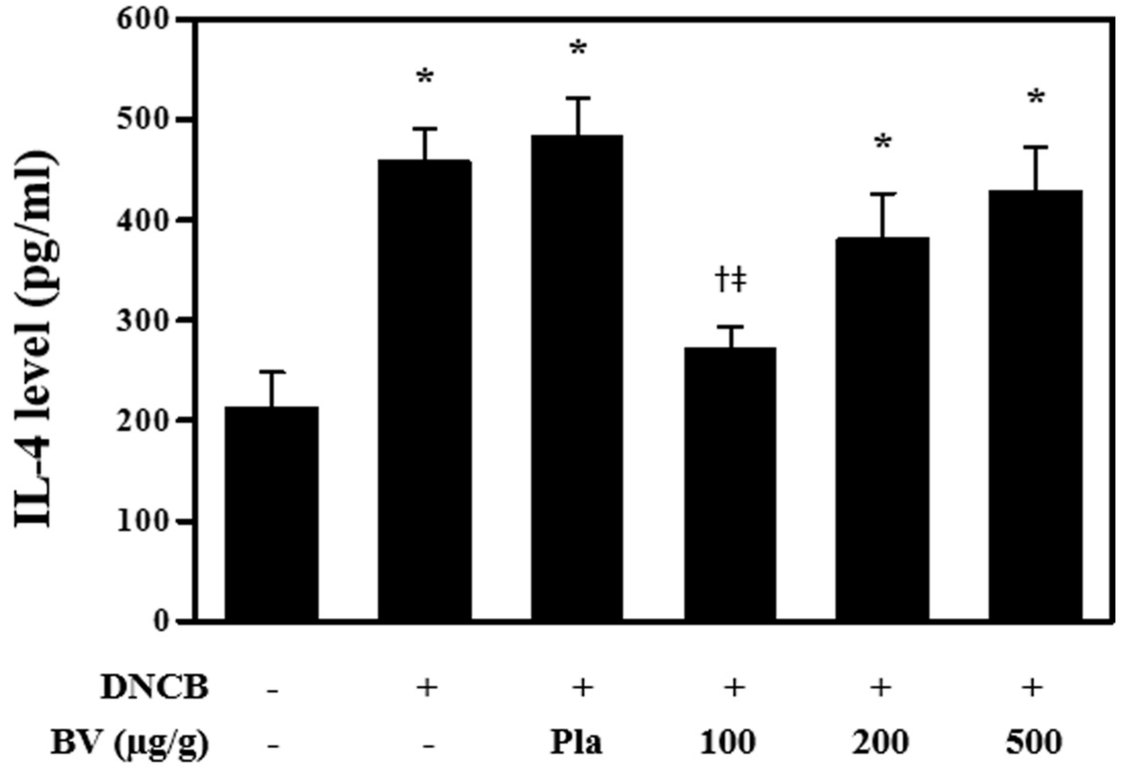

50 μm
20 μm
NC
DNCB
Pla
BV100
BV200
BV500

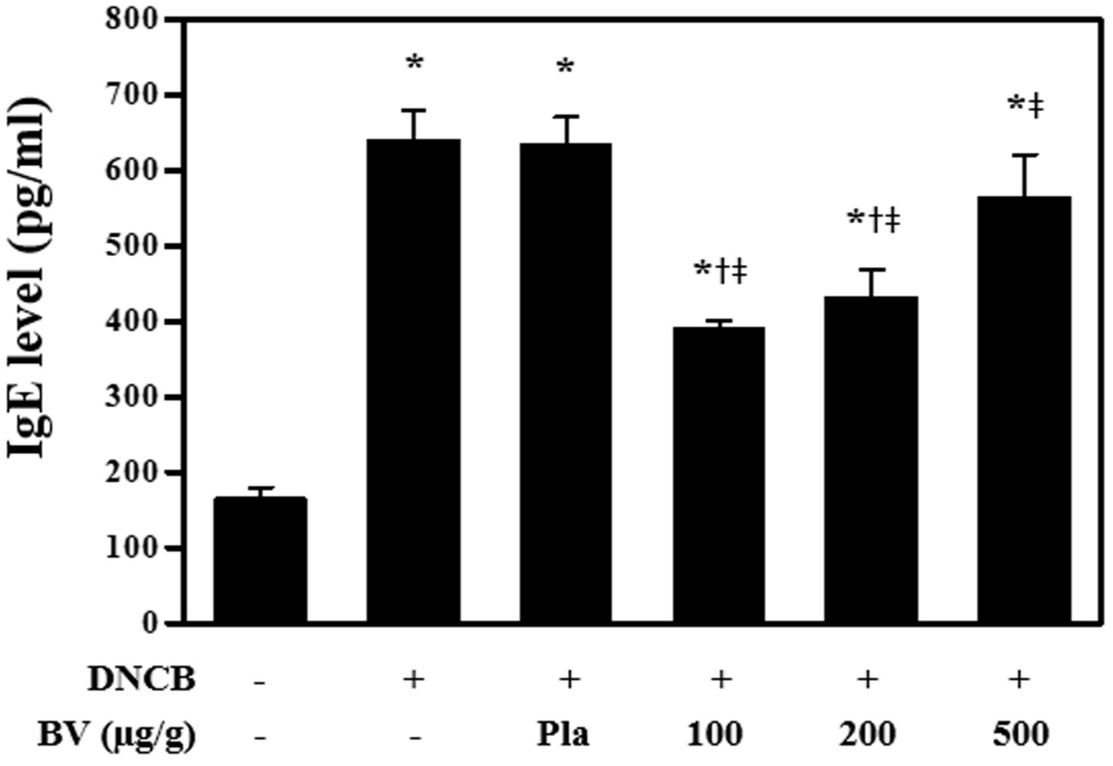
B

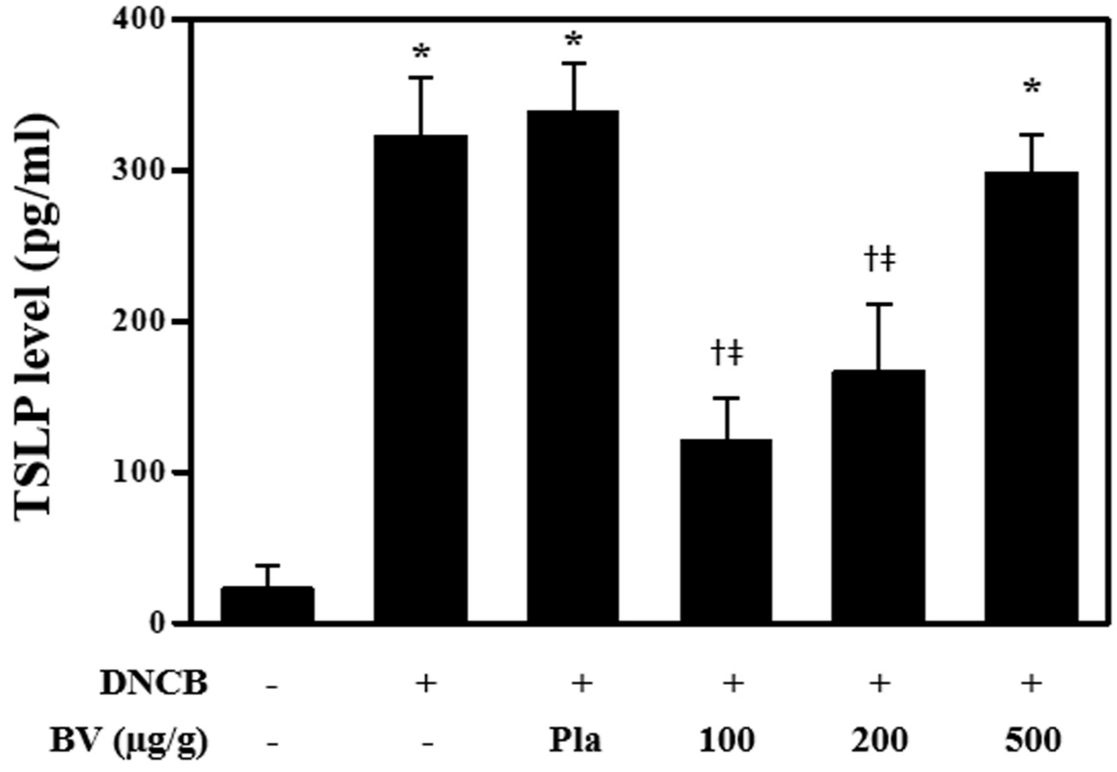

Mast cell infiltration /field
Degranulation /field
Degranulation rate (%)
DNCB - + + + + +
BV (μg/g) - - Pla 100 200 500
*
†‡
*†‡

A

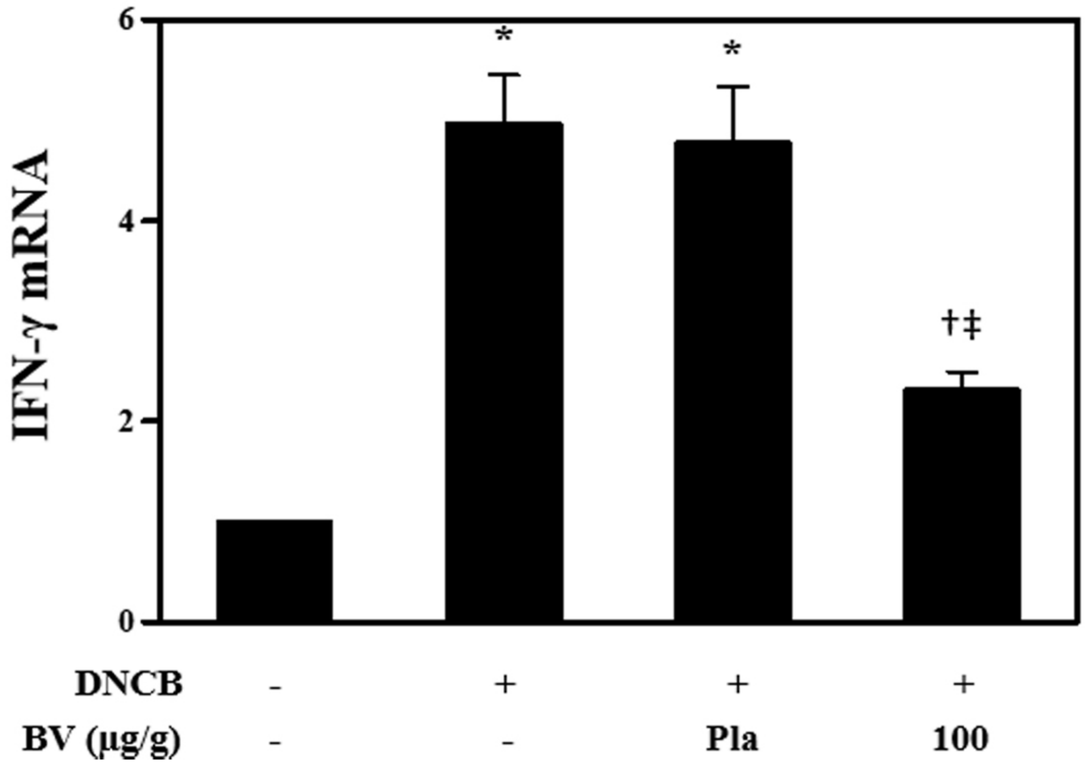

IFN-γ level (pg/ml)
800
700
600
500
400
300
200
100
0
*
*
†‡
*
*
DNCB - + + + + +
BV (μg/g) - - Pla 100 200 500

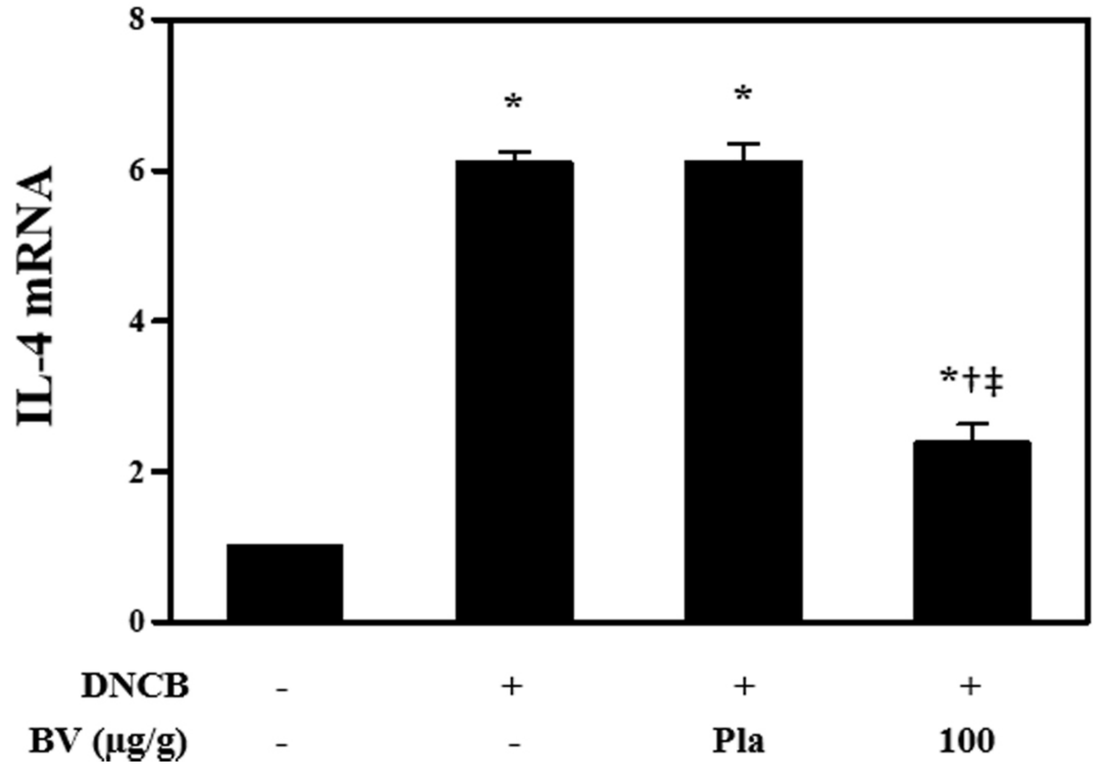

IL-4 level (pg/ml)
600
500
400
300
200
100
0
*
*
†‡
*
*
DNCB - + + + + +
BV (μg/g) - - Pla 100 200 500


IgE level (pg/ml)
800
700
600
500
400
300
200
100
0
*
*
*†‡
*†‡
*‡
DNCB - + + + + +
BV (μg/g) - - Pla 100 200 500

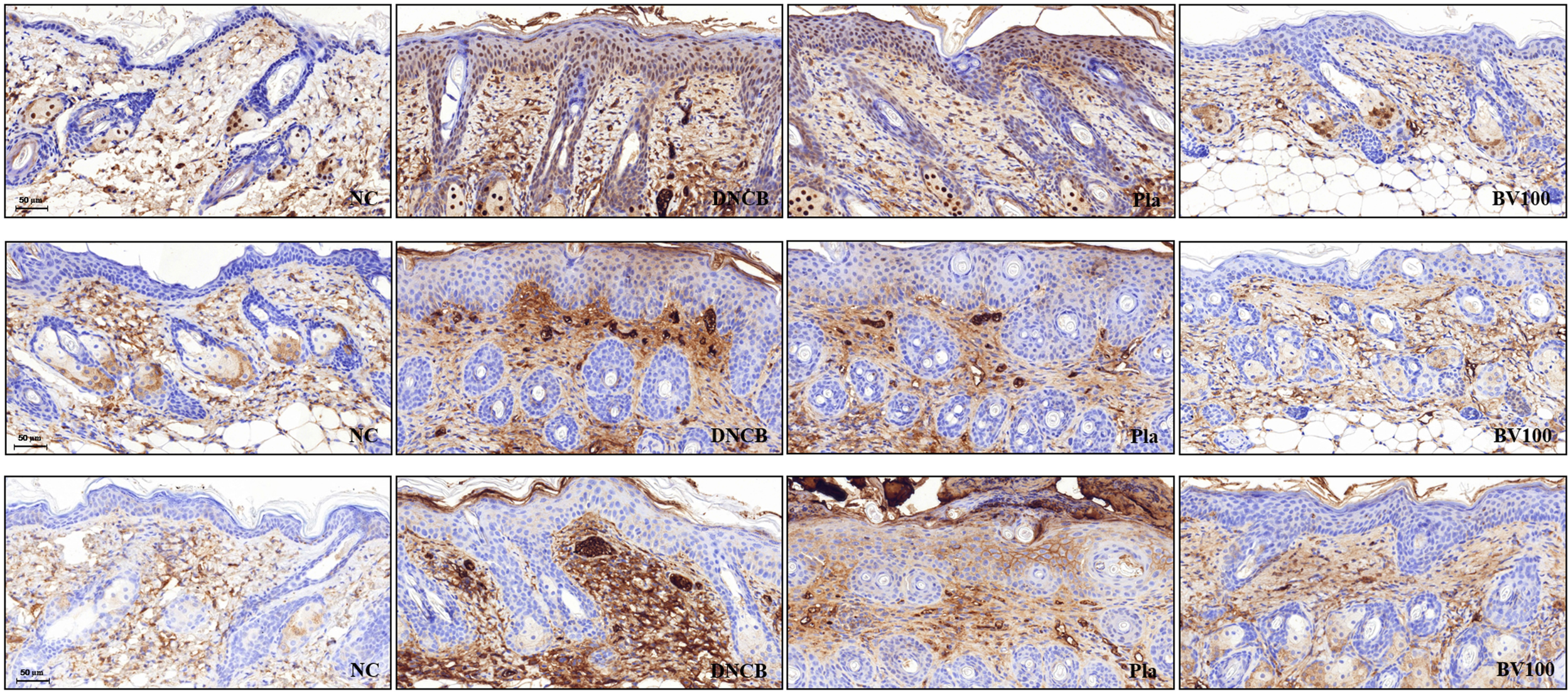

TSLP level (pg/ml)
400
300
200
100
0
*
*
†‡
†‡
*
DNCB - + + + + +
BV (μg/g) - - Pla 100 200 500

B

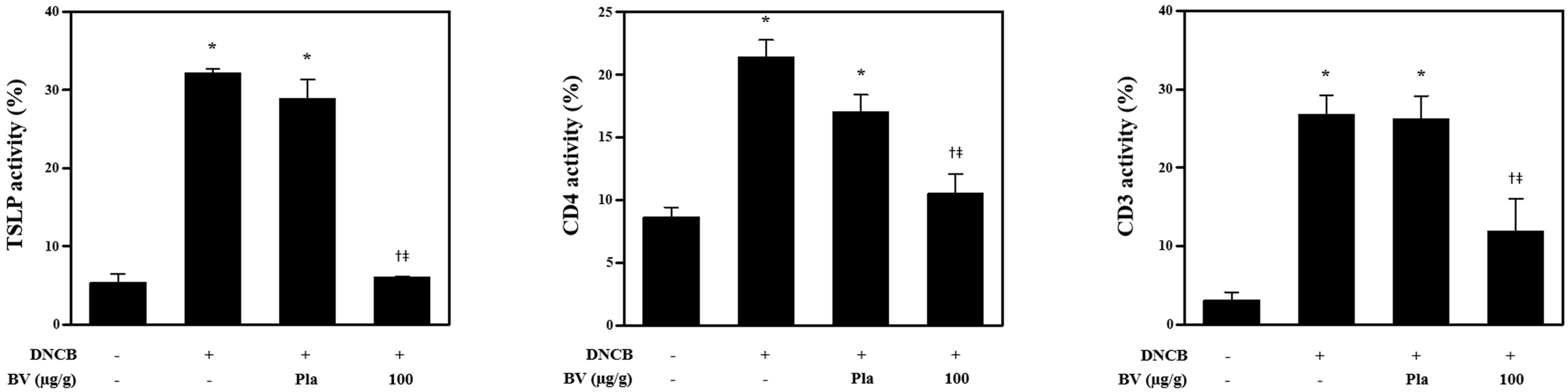

IFN-γ mRNA
6
4
2
0
*
*
†‡
DNCB - + + +
BV (μg/g) - - Pla 100


IL-4 mRNA
8
6
4
2
0
*
*
*†‡
DNCB - + + +
BV (μg/g) - - Pla 100

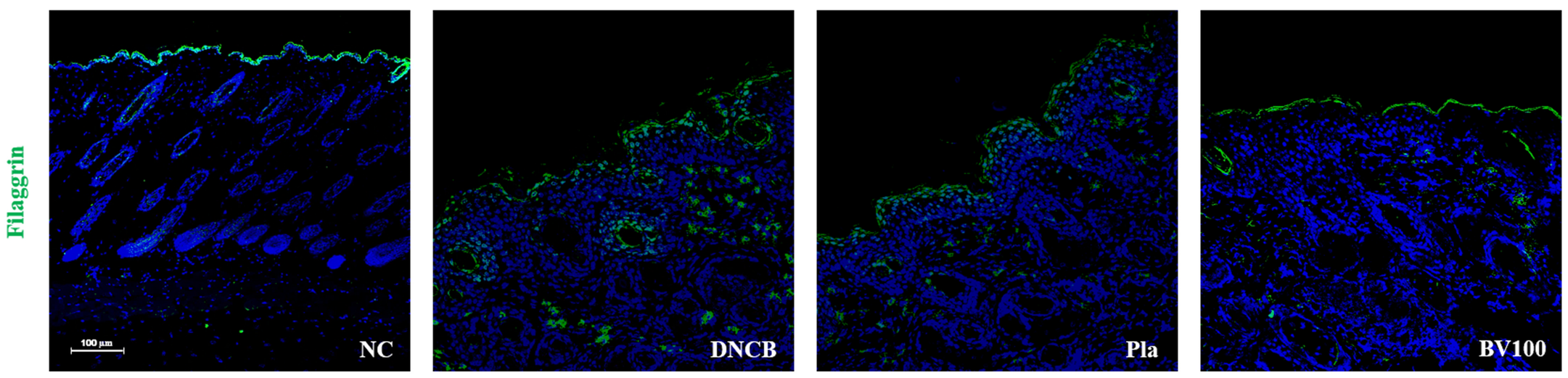
A


TSLP
CD4
CD3
NC
DNCB
Pla
BV100
50 μm

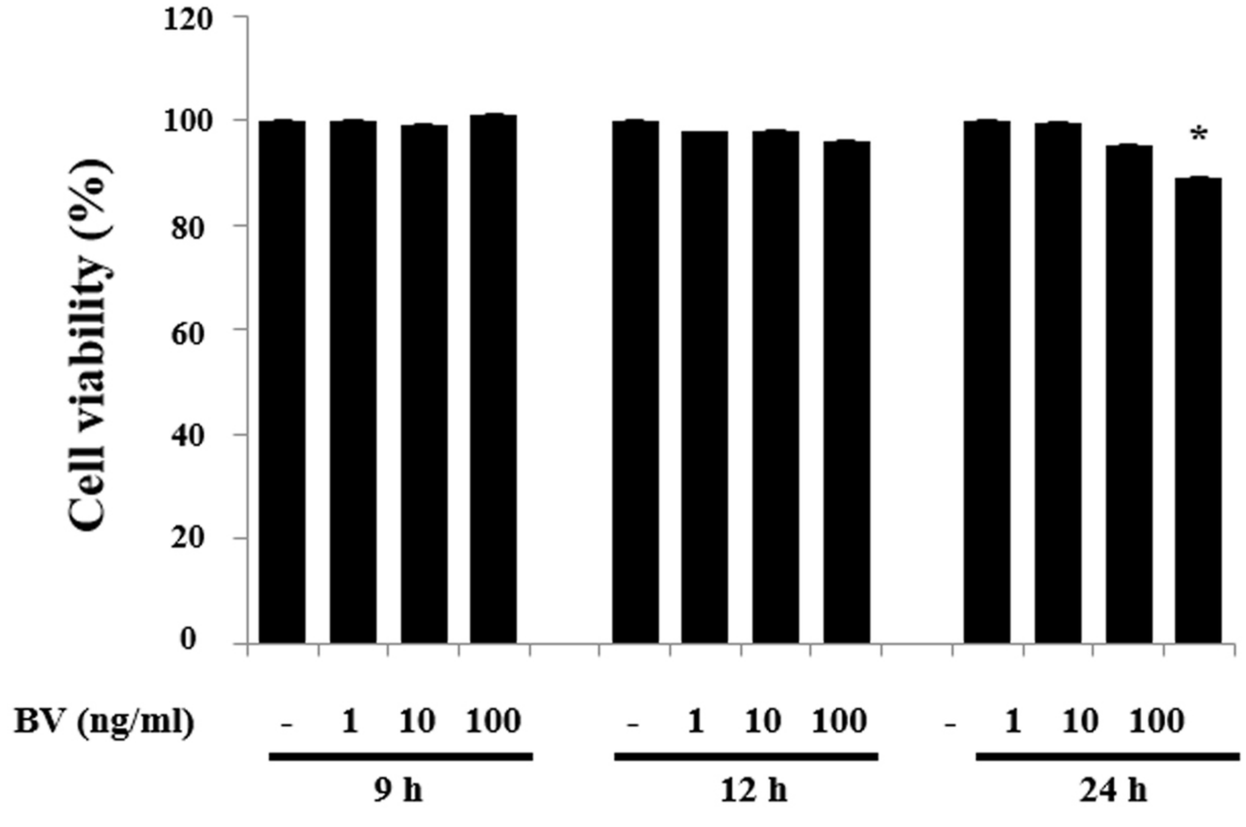
B


TSLP activity (%)
CD4 activity (%)
CD3 activity (%)
DNCB - + + +
BV (μg/g) - - Pla 100
*
†‡

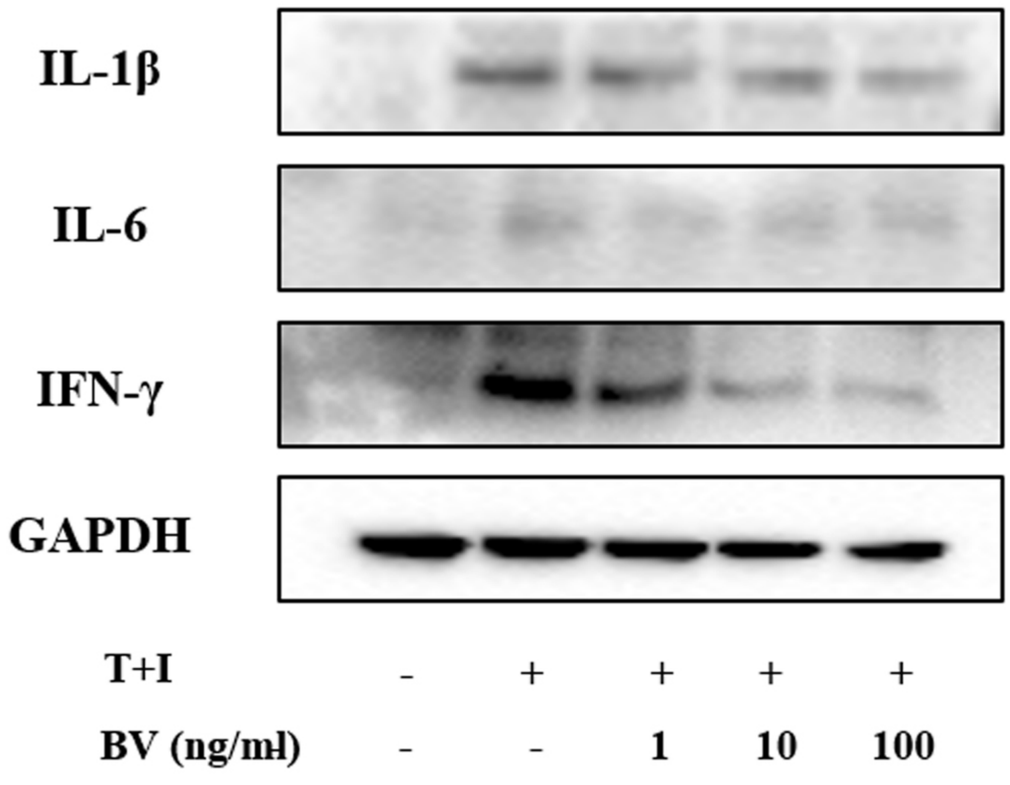
C


Filaggrin
NC
DNCB
Pla
BV100
100 μm

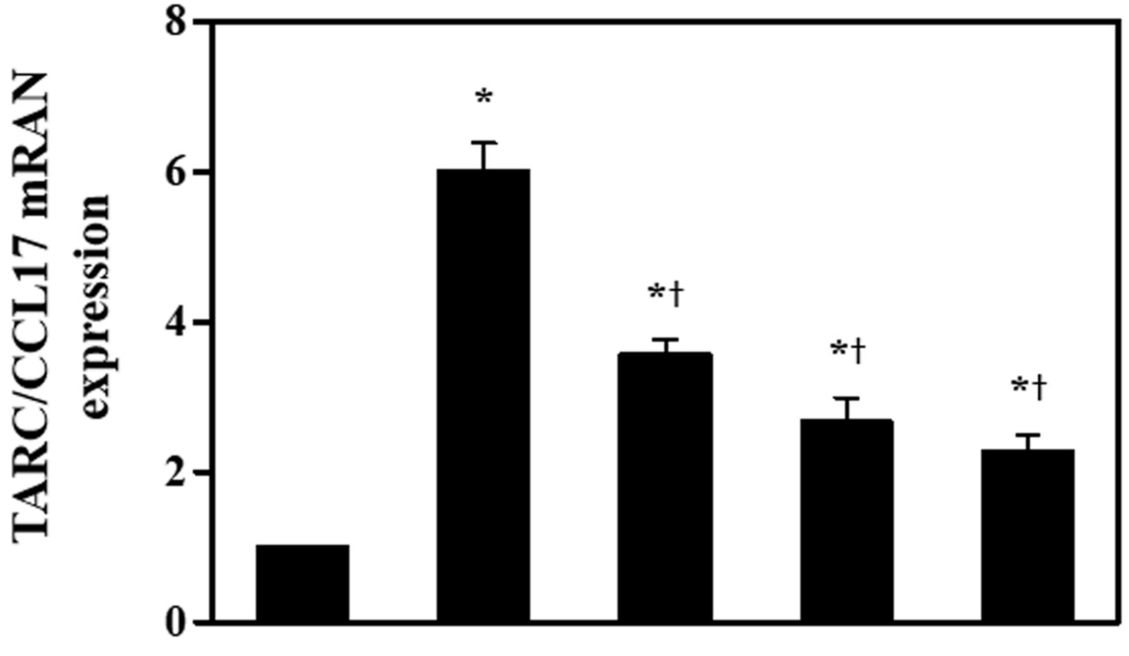
A

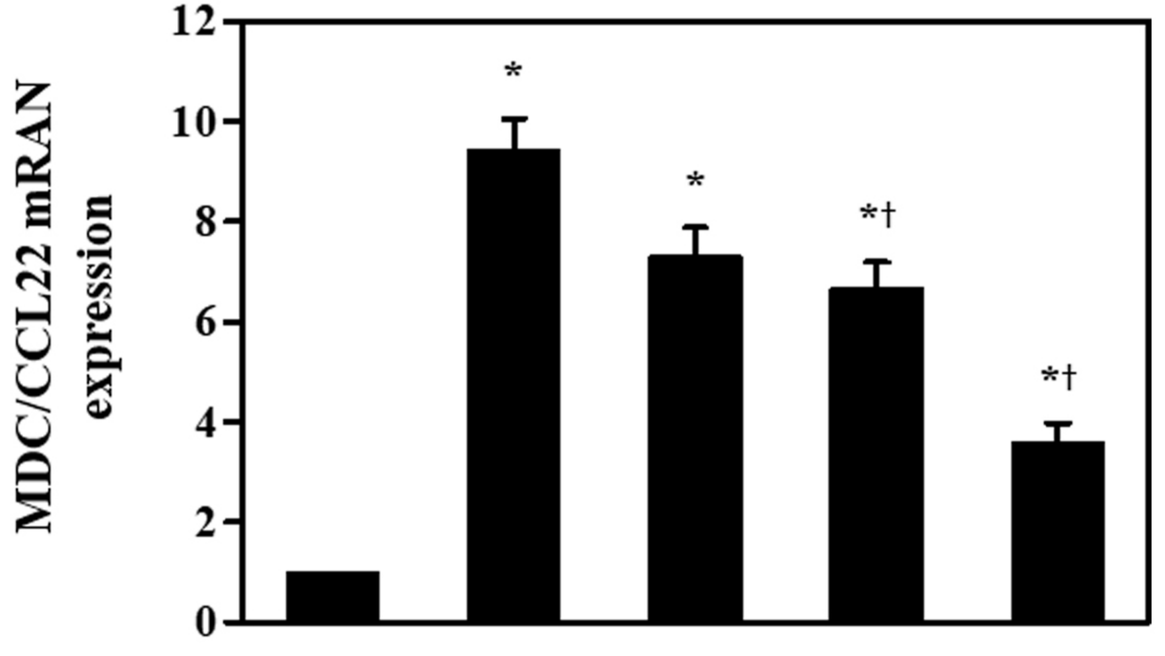

Cell viability (%)
120
100
80
60
40
20
0
*
BV (ng/ml)
- 1 10 100
- 1 10 100
- 1 10 100
9 h
12 h
24 h

B

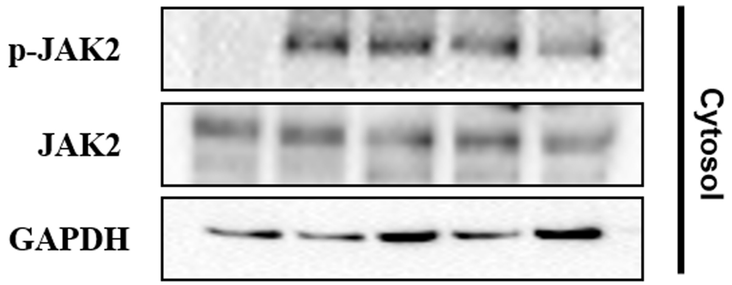

IL-1β
IL-6
IFN-γ
GAPDH
T+I - + + + +
BV (ng/ml) - - 1 10 100

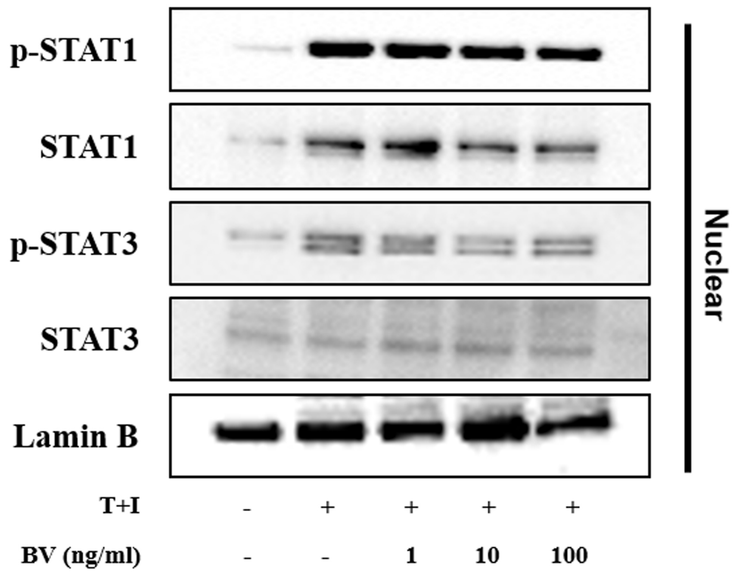
C


TARC/CCL17 mRAN expression
8
6
4
2
0
*
*†
*†
*†
T+I - + + + +
BV (ng/ml) - - 1 10 100

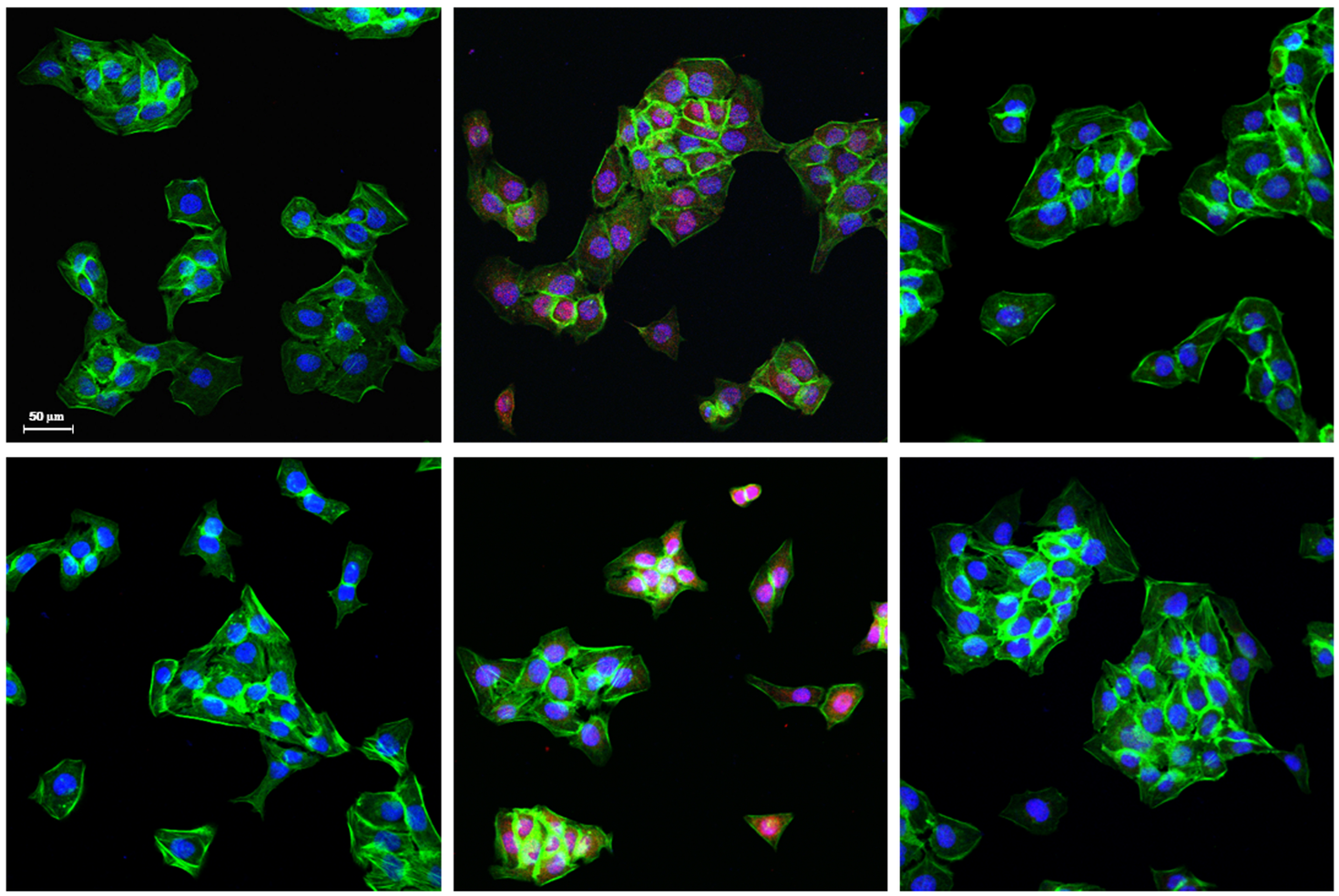

MDC/CCL22 mRAN expression
12
10
8
6
4
2
0
*
*
*†
*†
T+I - + + + +
BV (ng/ml) - - 1 10 100

A

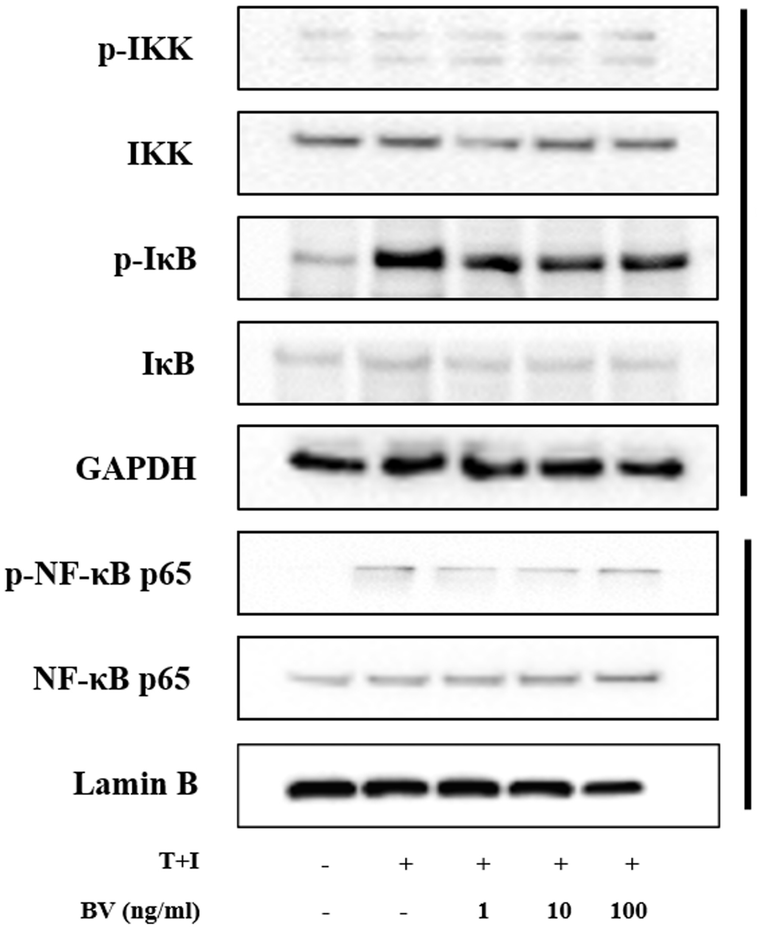

p-JAK2
JAK2
GAPDH
Cytosol
T+I - + + + +
BV (ng/ml) - - 1 10 100


p-STAT1
STAT1
p-STAT3
STAT3
Lamin B
Nuclear
T+I - + + + +
BV (ng/ml) - - 1 10 100

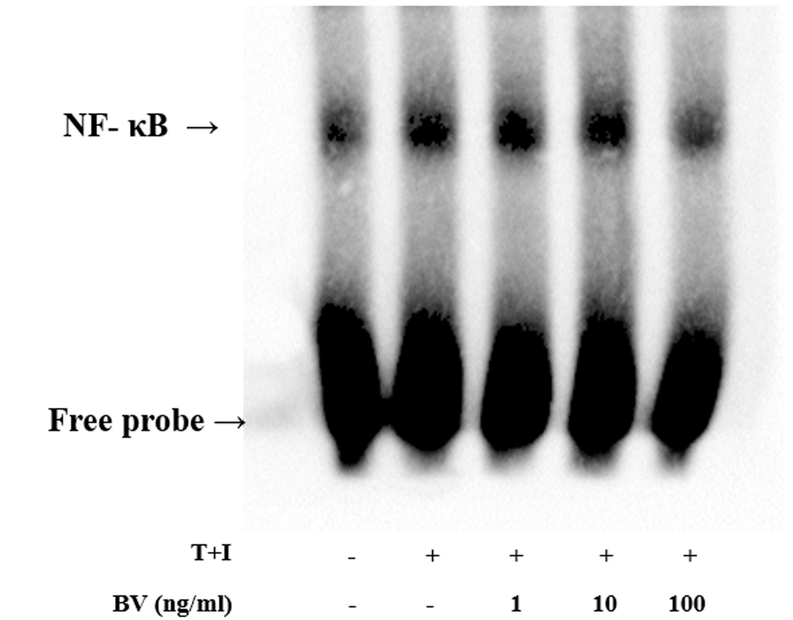
B


NC
T+I
BV100
p-STAT1
p-STAT3
50 μm

C


p-IKK
IKK
p-IκB
IκB
GAPDH
Cytosol
p-NF-κB p65
NF-κB p65
Lamin B
Nuclear
T+I - + + + +
BV (ng/ml) - - 1 10 100

D


NF- κB →
Free probe →
T+I - + + + +
BV (ng/ml) - - 1 10 100